2016

DEUTERIUM AND OXYGEN-18 DIFFUSION IN A CONFINED AQUIFER: A NUMERICAL MODEL OF STABLE ISOTOPE DIFFUSION ACROSS AQUITARD-AQUIFER BOUNDARIES

Benjamin J. Currens
University of Kentucky, ben.currens@uky.edu
Digital Object Identifier: http://dx.doi.org/10.13023/ETD.2016.334

STUDENT AGREEMENT:

I represent that my thesis or dissertation and abstract are my original work. Proper attribution has been given to all outside sources. I understand that I am solely responsible for obtaining any needed copyright permissions. I have obtained needed written permission statement(s) from the owner(s) of each third-party copyrighted matter to be included in my work, allowing electronic distribution (if such use is not permitted by the fair use doctrine) which will be submitted to UKnowledge as Additional File.

I hereby grant to The University of Kentucky and its agents the irrevocable, non-exclusive, and royalty-free license to archive and make accessible my work in whole or in part in all forms of media, now or hereafter known. I agree that the document mentioned above may be made available immediately for worldwide access unless an embargo applies.

I retain all other ownership rights to the copyright of my work. I also retain the right to use in future works (such as articles or books) all or part of my work. I understand that I am free to register the copyright to my work.

REVIEW, APPROVAL AND ACCEPTANCE

The document mentioned above has been reviewed and accepted by the student's advisor, on behalf of the advisory committee, and by the Director of Graduate Studies (DGS), on behalf of the program; we verify that this is the final, approved version of the student's thesis including all changes required by the advisory committee. The undersigned agree to abide by the statements above.

Benjamin J. Currens, Student

Dr. Alan E. Fryar, Major Professor

Dr. Edward W. Woolery, Director of Graduate Studies

DEUTERIUM AND OXYGEN-18 DIFFUSION IN A CONFINED AQUIFER: A NUMERICAL MODEL OF STABLE ISOTOPE DIFFUSION ACROSS AQUITARD-AQUIFER BOUNDARIES

THESIS

A thesis submitted in partial fulfillment of the
requirements for the degree Master of Science in the
College of Arts and Sciences
at the University of Kentucky

By

Benjamin J. Currens

Lexington, Kentucky

Director: Dr. Alan Fryar, Associate Professor of Earth and Environmental Sciences

Lexington, Kentucky

2016

ABSTRACT OF THESIS

DEUTERIUM AND OXYGEN-18 DIFFUSION IN A CONFINED AQUIFER: A NUMERICAL MODEL OF STABLE ISOTOPE DIFFUSION ACROSS AQUITARD-AQUIFER BOUNDARIES

The stable isotopes ^{2}H and ^{18}O, combined with noble gases and radioisotopes (e.g., ^{3}H, ^{14}C, ^{36}Cl), are used to infer groundwater age and climate during recharge. Flow regimes within low-velocity flowpaths and long residence times could allow an aquitard-aquifer diffusive flux to alter isotope abundance. Consequently, the diffusion of isotopes (e.g., ^{14}C, ^{2}H and ^{18}O) between aquifers and confining layers needs to be considered in such conditions. In this study, COMSOL Multiphysics was used to determine if diffusion of ^{18}O (and ^{2}H by proxy) from a bounding aquitard could explain observed downgradient enrichment of ^{2}H and ^{18}O within a regional aquifer. Using the geologic and hydraulic properties of the lower Wilcox aquifer of the Mississippi Embayment aquifer system in Missouri and Arkansas, the advection-dispersion equation was solved along a 1-D groundwater flow domain, coupled with a cross-contact aquitard-aquifer diffusive flux. Although the observed signal within the lower Wilcox was not matched, a sensitivity analysis indicated the importance of the isotope composition gradient between the aquifer and aquitard. Furthermore, groundwater velocity was suggested as a controlling influence on aquitard-aquifer exchange that could alter aquifer isotope composition.

KEYWORDS: Inferred Paleoclimate, Lower Wilcox, Regional Aquifer, Isotope Diffusion, Model

Benjamin J. Currens

27 July 2016

DEUTERIUM AND OXYGEN-18 DIFFUSION IN A CONFINED AQUIFER: A NUMERICAL MODEL OF STABLE ISOTOPE DIFFUSION ACROSS AQUITARD-AQUIFER BOUNDARIES

By

Benjamin J. Currens

Dr. Alan E. Fryar
Director of Thesis

Dr. Edward W. Woolery
Director of Graduate Studies

26 July 2016

ACKNOWLEDGEMENTS

This thesis would not have been possible without the prior work of Estifanos Haile. Furthermore, I would like to acknowledge the patience of my advisor, Alan Fryar, and committee: Audrey Sawyer, Thomas Parris, and Junfeng Zhu.

This material is based upon work supported by the National Science Foundation Graduate Research Fellowship under grant no. 3048109801.

TABLE OF CONTENTS

LIST OF TABLES

LIST OF FIGURES

Chapter One

1. Introduction

Isotopic composition of recharge waters is controlled by a variety of factors, including temperature (global and seasonal), proximity to source, altitude, and latitude. Precipitation is progressively depleted in heavier isotopes moving towards the poles and away from warmer, wetter regions around the tropics (Darling et al. 2005). The stable isotopic composition of precipitation can be influenced by kinetic fractionation or mixing at the ground surface, but once precipitation enters the soil zone as recharge, fractionation by evaporation is not possible and stable isotopic composition is generally considered conservative in non-geothermal waters. When combined with isotopic dating techniques (^{3}H, ^{4}He, ^{14}C, ^{36}Cl), ^{2}H and ^{18}O abundances can be used to infer the surface temperature at the time of groundwater recharge. For example, Plummer et al. (2012; Fig. 1) used combined techniques to identify waters recharged during the last glacial maximum within the Upper Patapsco aquifer of Maryland, and to demonstrate that these waters were isotopically distinct from water up and down-gradient.

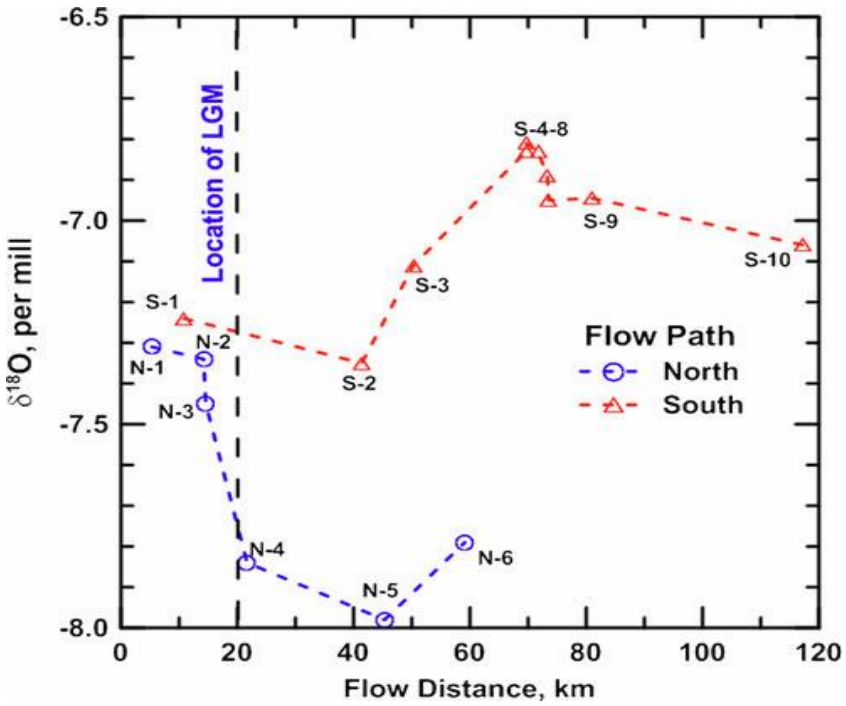

Figure 1 - $\delta^{18}O$ vs. flowpath distance in the Patapsco aquifer (Plummer et al. 2012). Note the inferred location of the Last Glacial Maximum (LGM) using combined isotope and dating methods.

In contrast, Haile (2011) documented increasing δ^2H and $\delta^{18}O$ values down-gradient along a regional flow path within the Wilcox aquifer, located in the Mississippi Valley of Missouri and Arkansas (Fig. 2). As modeling and solute concentrations indicated no significant mixing between the Wilcox and adjoining aquifers, and stable isotopes are considered conservative in the subsurface, this trend could only be a product of paleoclimate or a mechanism of further enrichment. Furthermore, as mixing acts to homogenize concentrations, enrichment or depletion along a flowpath would necessitate further fractionation. This is significant, as an unaccounted-for process altering isotopic abundance could lead to erroneous inferences about paleoclimate during groundwater recharge.

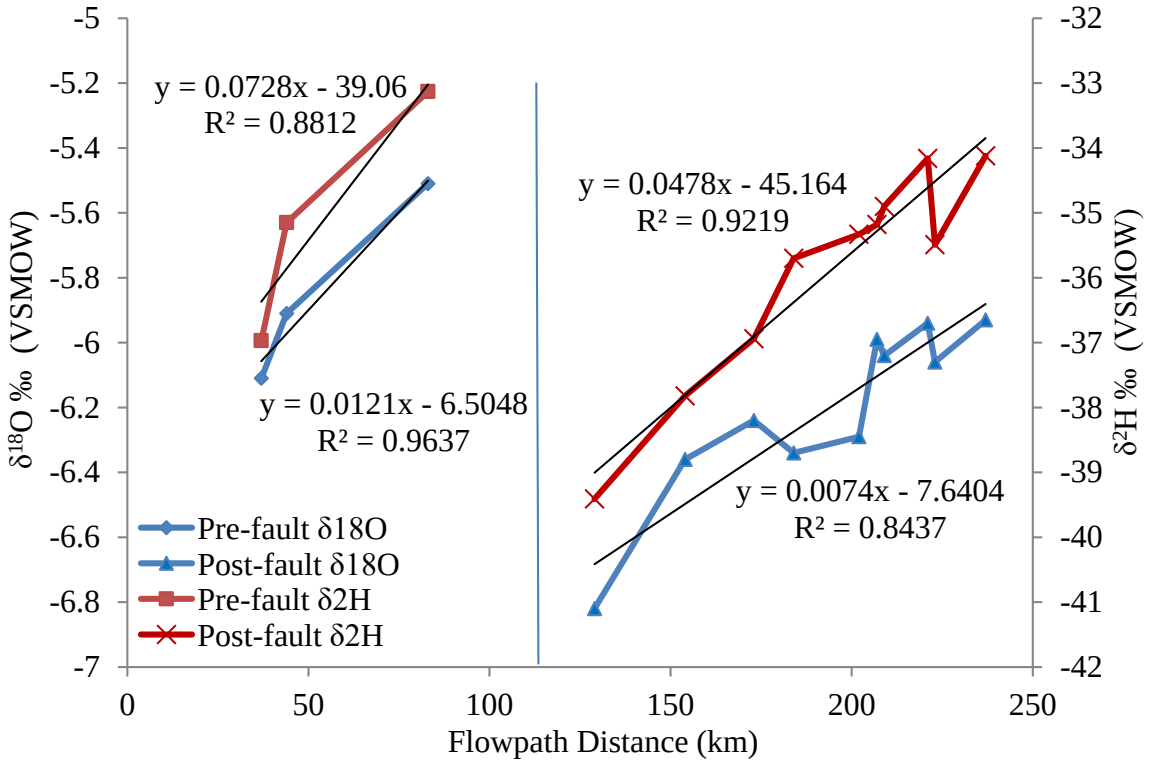

Figure 2 - $\delta^{18}O$ and δ^2H vs. distance along flowpath (after Haile [2011]). Vertical line (at 112 km) denotes inferred fault location.

LaBolle et al. (2008) provided evidence for diffusion as a mechanism for fractionation in the subsurface (Fig. 3). They demonstrated that diffusion of light isotopes from aquifers into slow-flow regions (aquitards) can produce apparent down-gradient enrichment in the aquifers. Additionally, they noted the importance of the isotopic concentration gradient:

diffusion of stable isotopes between newly recharged and older groundwater is unlikely if isotopic abundances are similar. However, LaBolle et al. (2008) did not address regional-scale flowpaths with a long residence time (e.g., 10^3 to 10^6 yr). Using an analytical model, Hendry and Schwartz (1988) explained down-gradient enrichment of ^{18}O along a regional-scale flowpath (~ 100 km) in the Milk River aquifer of southern Alberta by ^{18}O diffusion out of a bounding aquitard (Fig. 4).

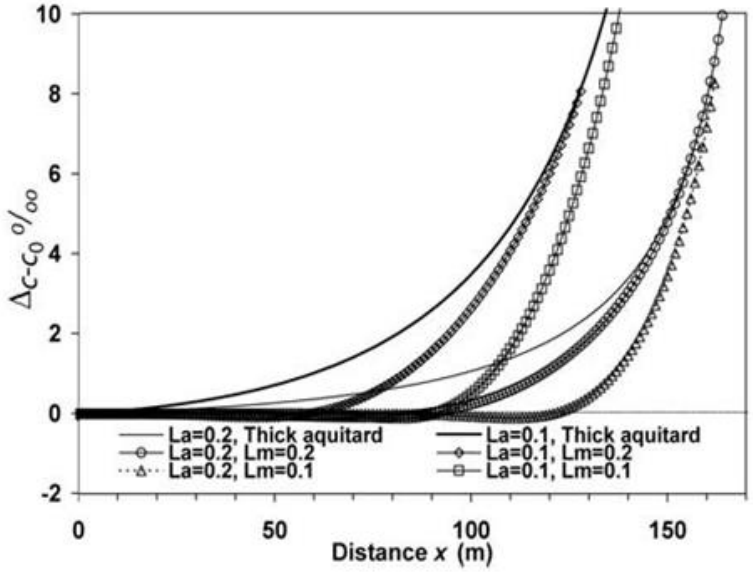

Figure 3 - Calculated isotopic enrichment under varying aquifer (La) and aquitard (Lm) thickness (LaBolle et al. 2008), where C_0 is the initial aquifer isotope composition and ΔC is the change in composition.

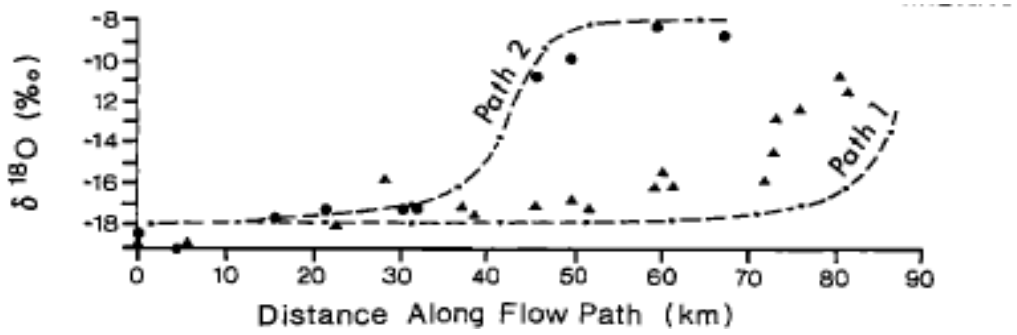

Figure 4 – $\delta^{18}O$ vs. flow path distance in the Milk River aquifer (Hendry and Schwartz 1988).

Given the findings of LaBolle et al. (2008) and Hendry and Schwartz (1988), this study addresses the following questions:

(1) How can diffusion of ^{18}O, and by proxy ^{2}H, between a confined aquifer and bounding aquitard influence stable isotope abundances along a regional flowpath?

(2) To what degree do residence time, aquifer and aquitard thickness, and isotopic gradient between an aquifer and aquitard influence aquifer isotope abundances?

(3) Is the apparent progressive enrichment of ^{2}H and ^{18}O down-gradient within the lower Wilcox aquifer (Fig. 2) the result of diffusion between the aquifer and a bounding aquitard?

To address these questions, a 1-D advection-dispersion transport model was constructed using COMSOL Multiphysics software (COMSOL, Inc., Burlington, MA) to calculate ^{18}O transport down the flowpath and between the aquifer and aquitard. To the extent possible, aquifer and aquitard hydraulic parameters were taken from observed values. Results were then compared to geologic, hydraulic, and geochemical data sets from the Wilcox aquifer for calibration.

Chapter Two

2. Background

2.1 Hydrostratigraphy and Groundwater Flow

The Wilcox Group is a Cenozoic sequence of fluviodeltaic sands, silts, and clays that underlies much of the Gulf Coastal Plain from Texas to Alabama and as far north as Missouri and Kentucky (Hart et al. 2008). It is overlain by the Claiborne Group and underlain by the Midway Group. The Wilcox Group is comprised of the Flour Island Formation, the Fort Pillow sand, and the Old Breastworks Formation in western Tennessee and eastern Arkansas (Hosman 1996). The Flour Island and the overlying Carrizo and Meridian sands in the lower Claiborne Group function as a single aquifer (lower Claiborne–middle Wilcox), which is overlain by the Cane River Formation and Zilpha Clay (the lower Claiborne confining unit). The Fort Pillow sand functions as the lower Wilcox aquifer (Hosman 1996). Aquifer stratigraphy varies from massive sands to interbedded sands and clays; periodic transgression is represented by flooding surfaces. Units generally strike northeast and dip south-southeast towards the Gulf of Mexico (Fig. 5; Haile 2011), but strike and dip vary spatially along the edge of the Mississippi Embayment.

Recharge of the lower Wilcox aquifer occurs at outcrop along the edge of the Mississippi Embayment or where the Wilcox is overlain by a thin cover of alluvium. Along the northwest margin of the embayment in Arkansas, recharge occurs along Crowley's Ridge. Groundwater flow is generally north to south parallel to the axis of the embayment. However, the potentiometric surface has likely been altered in some regions by pumping for municipal use. Modeled groundwater velocity within the confined aquifer ranged from 1.3×10^{-8} to 3.01×10^{-8} m/s, with greater velocities up-gradient (Haile 2011). Aquifer thickness and hydraulic properties vary vertically and areally, with thickness increasing predominantly north to south down-dip. Notably, the New Madrid Seismic Zone lies within the Mississippi Embayment and the aquifer has likely been displaced by faulting (Fig. 6). Haile (2011) indicated a fault perpendicular to flow direction ~ 110 km from Crowley's Ridge. The Mississippi Embayment Regional Aquifer System (MERAS) model (Clark and Hart 2009) treated cross-fault flow as impeded, which suggests that the aquifer transitions from unconfined to confined proximal to this fault. However, no prior work appears to have examined cross-formational flow along the fault plane identified within Haile's study.

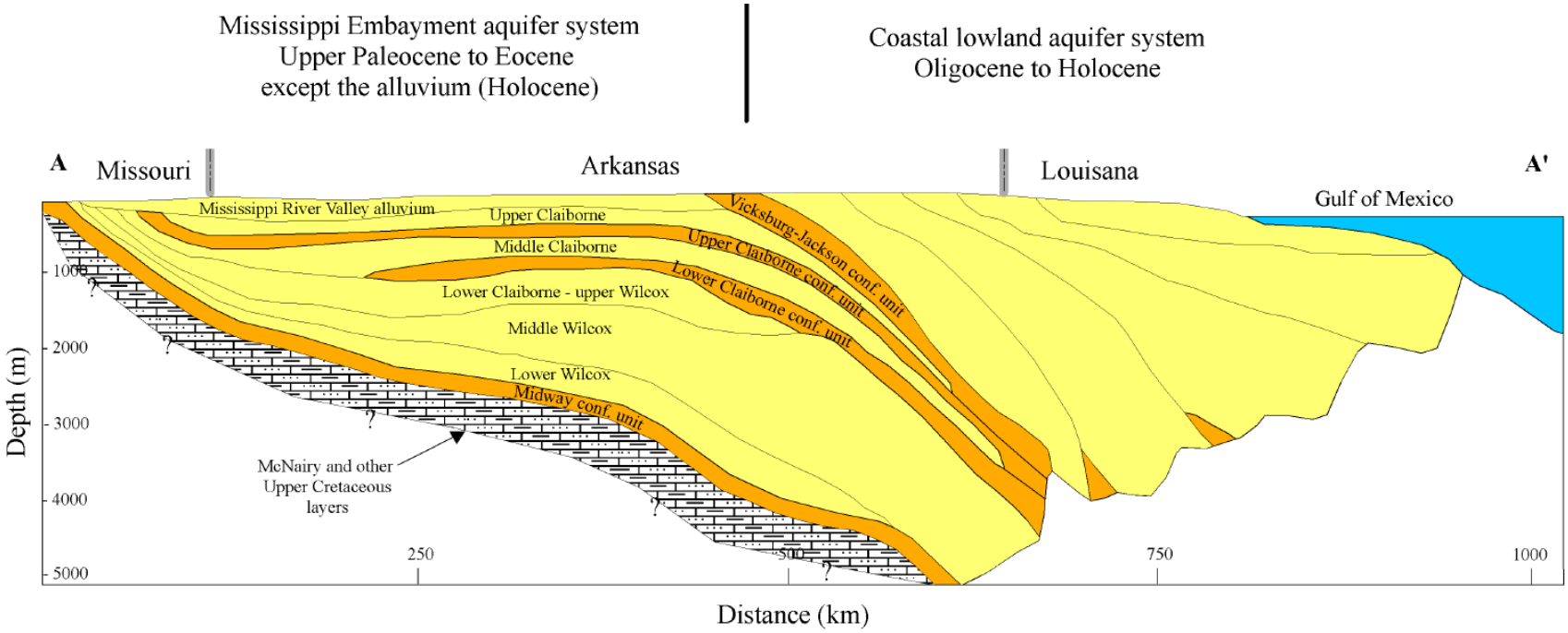

Figure 5 - Wilcox cross-section from north to south (Haile [2011], modified from Williamson and Grubb [2001]). Cross-section location shown on Figure 6.

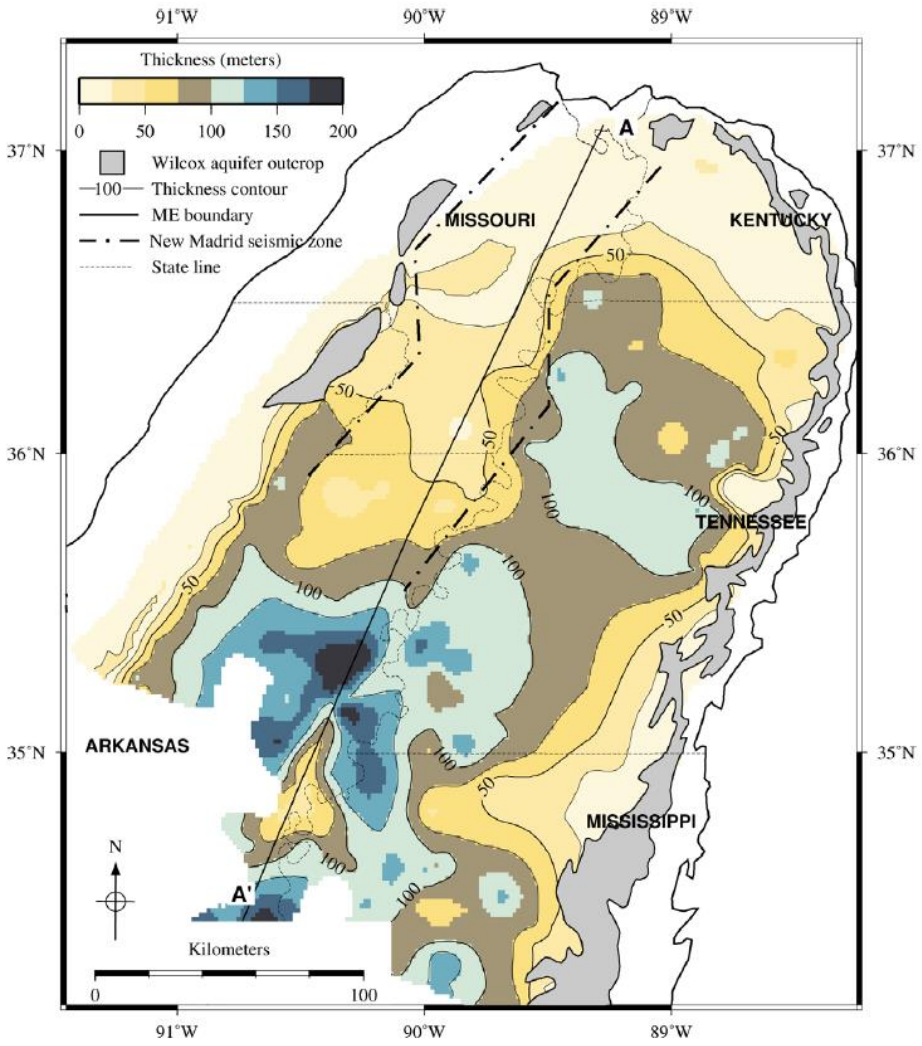

Figure 6 - Isopach map of the Wilcox Group (Haile 2011).

2.2 Paleoclimate

Chlorine-36 data suggest groundwater ages of ~150 to 700 kyr within the down-gradient (confined) lower Wilcox (Haile 2011). For this period in the middle Mississippi Valley, studies have addressed relative humidity (via modeling based on stable isotopes within sub-fossil wood [Voelker et al. 2015]), modeled precipitation (Bromwich et al. 2005; Kim et al. 2006), palynology and ecological succession (Davis and Shaw 2001; Williams et al. 2001), sea level (Muhs et al. 2003a), paleopedology and thermoluminescence (Markewich et al. 1998; Rovey and Balco 2011; Forman and Pierson 2002), loess deposition (Muhs et al. 2003b) and speleothem $\delta^{18}O$ (Denniston et al. 2007; Dorale et al. 1998; Harmon and Schwarcz 1981). However, there is a dearth of data for both

precipitation and its isotope abundance, which reflects a lack of proxies (in particular, speleothems) within the region older than 75,000 years before present (ybp).

2.2.1 Isotope signals

Using paired speleothem calcite $\delta^{18}O$ values and inclusion water $\delta^{2}H$ values with U/Th dating, Harmon and Schwarcz (1981) calculated paleotemperature at six sites across the Caribbean and North America. They found that temperatures calculated using the temperature dependence of ^{18}O fractionation between calcite and water (from O'Neil et al. (1969); $10^3 \ln\alpha_{c\text{-}w} = 2.78\times10^6\ T^{-2} + 2.89$, where α is the fractionation factor) were < 0 °C (i.e., too low for calcite precipitation). They then suggested that the current GMWL does not accurately represent the $\delta^{2}H$-$\delta^{18}O$ relationship during the growth of these speleothems. Harmon and Schwarcz (1981) argued that speleothem drip waters in temperate regions of North America are isotopically similar to precipitation, but Wackerbarth (2012) noted that a variety of factors could alter isotopic composition. Conversion from paleowater to precipitation $\delta^{18}O$ values requires independent data on temperature (Friedman and O'Neil 1977) and humidity [Wackerbarth 2012]), which are not available for the time period of interest in the current study area. Of the sites sampled by Harmon and Schwarcz (1981), a cave in Kentucky was closest to the lower Wilcox recharge area. The inferred $\delta^{18}O$ values based on the modern GMWL and the authors' inferred paleo-GMWL are shown in Figure 7.

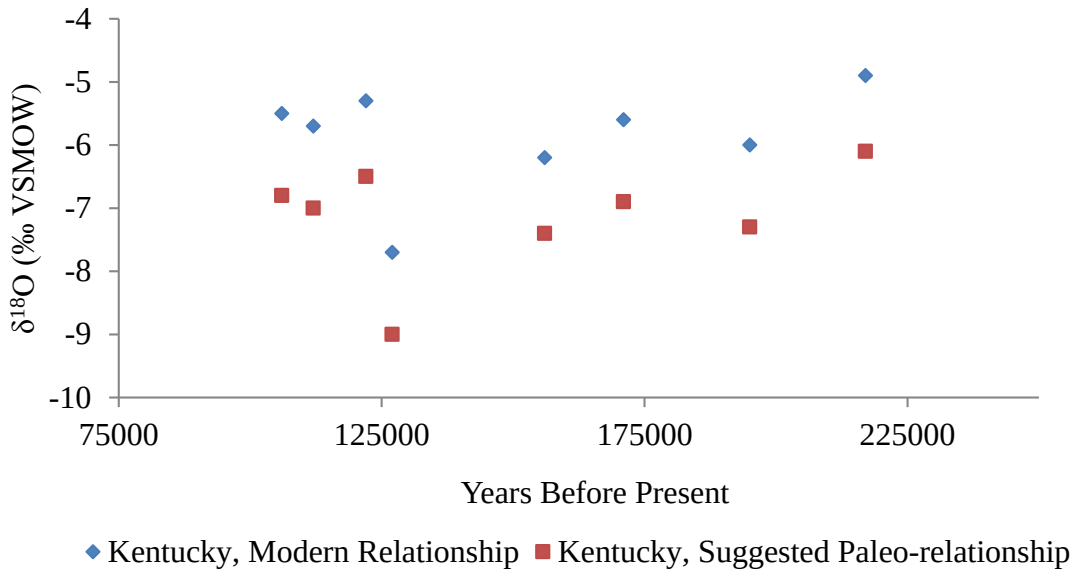

Figure 7 - Calculated inclusion-water $\delta^{18}O$ (SMOW) using modern $\delta^{2}H$–$\delta^{18}O$ relationship (blue) and proposed paleorelationship (red) (U/Th dated; Harmon and Schwarcz 1981).

Dorale et al. (1998) examined speleothems within several caves in central and eastern Missouri. The data include calcite $\delta^{18}O$ with U/Th dating and do not include drip water $\delta^{18}O$, but they do represent trends in isotope values proximal to the recharge area of the lower Wilcox and are coupled with ice volume estimates (Fig. 8).

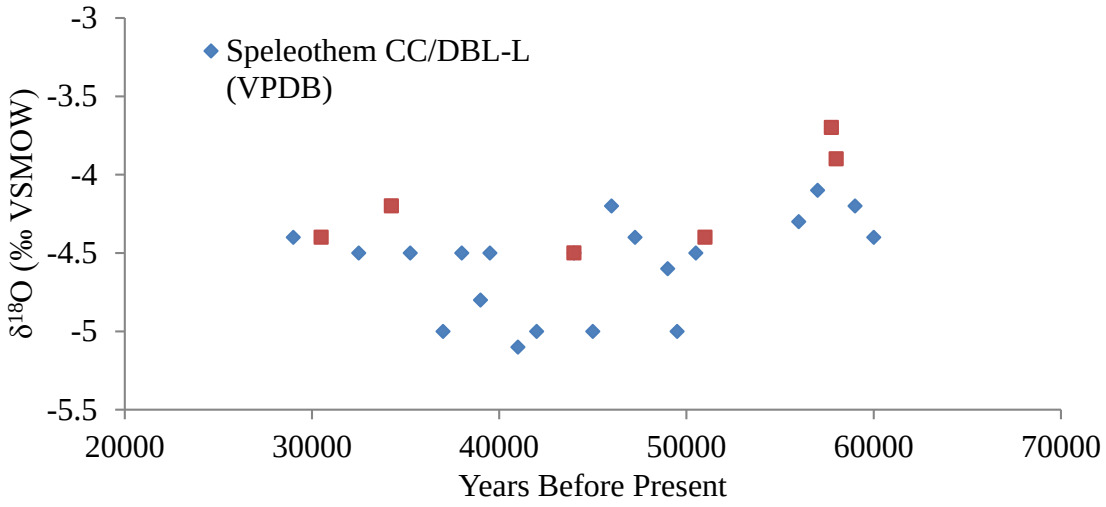

Figure 8 - Speleothem $\delta^{18}O$ vs. years before present (Dorale et al. 1998).

2.2.2 Reconstruction

For the period of interest (from present to ~ 250,000 ybp), the oldest datable unit in the middle Mississippi Valley is the Crowley's Ridge loess, which was deposited between 274 and 250 ka (Markewich et al. 1998, Forman and Pierson 2002). With the onset of the Illinoian glacial period tied by multiple methods to ~ 190 ka, the Crowley's Ridge loess and coeval till deposition further north likely represent the advance of a lobe of the Laurentide ice sheet during a pre-Illinoian event (Rovey and Balco 2011). However, no isotope data are available within the region prior to 217 ka (the Crowley's Ridge loess was dated by luminescence techniques), and while a negative slope is evident from 217 to 195 ka (Fig. 7), the $\delta^{18}O$ values are only suggestive of glaciation. Sea level was close to present for some period between 230 and 220 ka (Muhs et al. 2003), which is consistent with interglacial conditions.

Generation of the Yarmouth paleosol during the Illinoian and interglacial period (potentially ≥ 218 to 154 ka [Forman and Pierson 2002]) suggests wetter, warmer conditions early in the Illinoian. However, because the Yarmouth paleosol lies within the

upper section of the Crowley's Ridge loess, the variety of dates for Crowley's Ridge deposition confounds estimates of the date and duration of pedogenesis. Forman and Pierson (2002) placed deposition of the loess as early as 264 ka, while Markewich et al. (1998) placed deposition prior to 200 ka. Both studies agreed that loess deposition had occurred by 200 ka, which is supported by till (Macon Member) deposition north of the recharge area around 196 ka (Rovey and Balco 2011). Although a variety of dating methods have been used for paleoclimate studies in the region (e.g., ^{14}C, thermoluminescence, infrared stimulated luminescence), definite demarcation of climate based on loess deposition or pedogenesis alone is difficult.

Deposition of the Loveland 1 loess (Rodbell et al. 1997), a maximum sea-level low stand at 135 ka, and general low sea level from 175 to 130 ka (Dyke and Prest [1987] in Forman and Pierson [2002]) all coincide with the Illinoian glacial period from 191 to ~ 130 ka (Markewich et al. 1998). The onset date (191 ka) is in agreement with marine isotope stage 6 (Markewich et al. 1998). The decreasing $\delta^{18}O$ composition for speleothem inclusion values from Harmon and Schwarcz (1981) also agrees with Illinoian glaciation between 175 and 130 ka (Fig. 7).

Between 138 and 60 ka, silt deposition ceased and the Sangamon paleosol formation began (Markewich et al. 1998; Forman and Pierson 2002; Rodbell et al. 1997), suggestive of a wetter, warmer climate. This period was interrupted by loess deposition (Loveland 2–3), associated with drier conditions, from ~ 115 to ~ 70 ka (Rodbell et al. 1997). During loess deposition, sea level fluctuated between ~ 10 and 50 m below present (Dyke and Prest [1987] in Forman and Pierson [2002]). The boundaries of the Sangamon are contentious, with inferred ages as young as 31 ka (based on ^{14}C [Forman and Pierson 2002]). A period of warmer (and potentially wetter) conditions around 120 ka is further supported by a meltwater pulse recorded by $\delta^{18}O$ in Gulf of Mexico sediments (Joyce et al. 1993) and by near-modern sea levels (Dyke and Prest [1987] in Forman and Pierson [2002]). This pulse is likely proximal to the glacial-interglacial transition following the Illinoian period. A stark increase in $\delta^{18}O$ observed by Harmon and Schwarcz (1981) (Fig. 7) indicates changing conditions between 130 and 125 ka.

Coinciding with the onset of the Wisconsinian period, aeolian deposition of the Roxana silt within the region occurred between 60 and 26 ka (Markewich et al. 1998). Sea level was 5 to 8 m above present by 25 ka (Muhs et al. 2003), but fell to a low stand of ~120 m below present around 22 ka. Proximity to the Laurentide ice sheet (Williams et al. 2001; Rovey and Balco 2011) and topographic forcing along its southern margin (Bromwich et al. 2005) have been suggested to affect both seasonal variation and annual precipitation. This is supported by vegetation dissimilarity increasing with distance southward from the Laurentide margin (Williams et al. 2001). Palynology indicates peak vegetation dissimilarity between 16–14 ka, with spruce becoming common within the region by 11 ka and a shift towards modern vegetation beginning at 9 ka (Williams et al. 2001).

Combined with precipitation and relative humidity reconstruction, this suggests drier conditions (0.65–0.95 m/yr annual precipitation) than modern in the study area between 16 and 11 ka (Voelker et al. 2015).

Furthermore, modeling suggests that juxtaposition of cold air near the ice sheet and warmer, moist air from the Gulf Coast likely caused increased precipitation immediately adjacent to the ice sheet (Bromwich et al. 2005) and decreased precipitation further south. Bromwich et al. (2005) also found that monsoonal patterns of precipitation during summer months were possible during the Last Glacial Maximum (LGM). Bromwich et al. (2005) modeled a summer air temperature of 18 °C at the LGM (versus a modern value of ~ 24 °C at Malden, MO [Missouri Climate Center 2016]) and annual precipitation of 1.02 m/yr. Summer and winter LGM precipitation were calculated to be 2–4 mm/day and 1–4 mm/day, respectively, a change from modern observed values of 0 to -0.5 mm/day in the winter and -0.4 to -0.5 mm/day in the summer (Kim et al. 2006). Taken together, this could indicate reduced overall precipitation combined with seasonal monsoonal rains. However, Kim et al. (2006) noted that the overall change in precipitation is roughly zero when lower evaporation rates are accounted for. Current average annual precipitation for the region is 0.89–1.32 m/yr, and potential evapotranspiration is 0.84–1.14 m/yr (Haile 2011).

Chapter Three

3. Methods

3.1 Model Design

The model domain was limited to the confined section of the lower Wilcox, which was suggested by Haile (2011) to span ~ 175 km, beginning immediately downgradient of a fault displacing the Wilcox Group near New Madrid, Missouri (Fig. 9). Water mass and isotope fluxes were introduced along the upper boundary and the lower boundary was open to both. All other boundaries were no-flow. $^{18}O/^{16}O$ ratio and transport down-gradient were then calculated using COMSOL's combined advection-dispersion/ diffusion function. An additional ordinary differential equation was created along the entire length of the domain to represent a diffusive flux between the aquitard and aquifer. As the direction of aquifer-aquitard isotope exchange was determined by the concentration gradient, diffusion could occur both into and out of the aquifer. The model assumes that the aquifer is isotropic and well mixed transverse to flow; the aquitard is well mixed in the transverse and longitudinal directions; there is little to no fluid flow across the aquitard-aquifer contact; and groundwater flow can be treated as 1-D along the longitudinal axis of the aquifer.

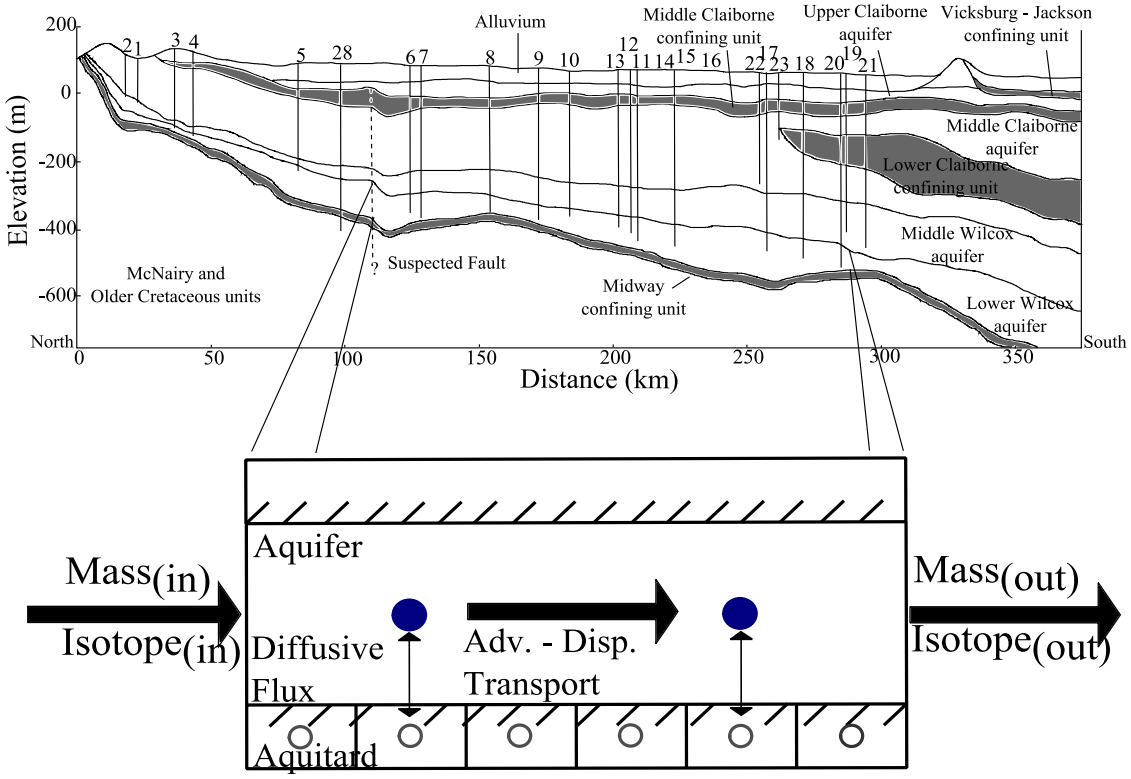

Figure 9 - Cross-section parallel to flowpath (north - south); note fault (dashed line) at ~ 110 km (from Haile [2011] after Hart et al. [2008]), sampled well locations, and model concept. Model domain spans flowpath from fault to last sampled well within the lower Wilcox (#20). Note the diffusive flux is isotope gradient controlled between the aquifer (blue dot) and aquitard (hollow dot).

3.1.1 Groundwater Flow and Calibration

Mass flux at recharge was adjusted to match the head gradient observed by Haile (2011; Appendix A) and the order of magnitude of groundwater velocity calculated from ^{36}Cl residence times. As a zero-head condition was chosen for the lower boundary, observed head in post-fault wells from Haile (2011) was shifted to allow direct comparison between observed and model output. Beginning with effective recharge of 0.151 m/yr, the recharge flux within the model was adjusted to approximate the shifted, observed head gradient (Fig. 10) and agree with residence time-derived groundwater velocity (10^{-8} m/s). A recharge flux of 0.14 m/yr was selected for aquifer porosity of 0.15 and a recharge flux of 0.1395 m/yr was selected for aquifer porosity of 0.225. Slope varied from observed linear best fit by 0.01 m/km and groundwater velocity varied from average modeled lower Wilcox by 1.95×10^{-9} and 8×10^{-9} m/s for the different recharge fluxes.

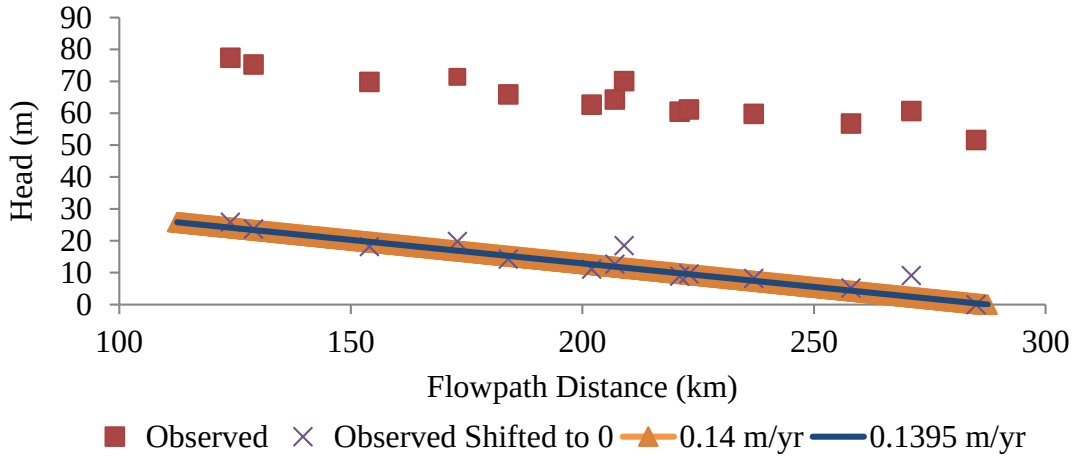

Figure 10 - Head vs. post-fault flowpath distance.

3.1.2 Isotope distribution

Isotope transport is solved within COMSOL using a combined advection-dispersion and diffusion equation with an additional cross-contact diffusive flux:

$$\theta_s \frac{\partial C_x}{\partial t} = \left(-D_{D,x} + \theta \tau_{L,i} D_{L,x}\right) \frac{\partial^2 C_i}{\partial x^2} - u \frac{\partial C_i}{\partial x} \pm diffusive\ flux \pm reaction\ and\ sorption\ terms \quad (1)$$

where $\left(-D_{D,x} + \theta \tau_{L,x} D_{L,x}\right) \frac{\partial^2 C_x}{\partial x^2}$ is the dispersion-diffusion term, $u \frac{\partial C_x}{\partial x}$ is the advection term and θ_s is aquifer porosity. Within $\left(-D_{D,x} + \theta \tau_{L,x} D_{L,x}\right)$, D_D is the species diffusion coefficient, θ is liquid volume fraction (equal to porosity under saturated conditions), τ is tortuosity, and D_L is longitudinal dispersivity (m^2/s); x (m) indicates distance down the flowpath. No reaction or sorption terms are anticipated given the species involved. Diffusive transport within a porous medium, although small, must also account for tortuosity by calculating effective diffusion. Within COMSOL effective diffusion is calculated as:

$$D_e = \emptyset_L \tau_L D_D, \quad (2)$$

where D_D is the diffusion coefficient for the species, ϕ_L is the effective porosity, and τ_L is the tortuosity of the media. For saturated porous media, τ_L is approximated as $\theta^{1/3}$.

3.1.3 Aquifer-aquitard diffusive flux

The flux (*f*) between the aquifer and aquitard (Fig. 9) is assumed to follow Fick's law:

$$f = -D \frac{(C_{f_i} - C_{t_i})}{\Delta y}, \quad (3)$$

where D is the diffusion coefficient of the species, C_{f_j} is the isotope concentration within the aquifer, C_{t_i} is the isotope concentration within the aquitard, and Δy is the distance across the aquifer-aquitard contact; i indicates node. Within COMSOL, the diffusive flux with respect to time was calculated as:

$$\frac{\partial C_t}{\partial t} = \frac{-D}{\Delta y \emptyset_t b_t} (C_{t_i} - C_{f_i}), \quad (4)$$

where C_{t_i} is the aquitard isotope concentration, C_{f_i} is the aquifer isotope concentration, $\emptyset_t$ is aquitard porosity, b_t is aquifer thickness, and Δy is the aquitard interaction thickness (nodal spacing).

3.2 Boundary Conditions

Bounding aquitards were represented by no-flow boundaries. A mass flux was introduced at the upper boundary with groundwater flow moving from the upper to lower boundary. The lower boundary was open for mass. The upper boundary (herein referred to recharge) consisted of a time-dependent function for the isotope flux and a mass flux representing recharge across the study period. The initial model concept was intended to simulate glacial-interglacial variation in recharge, and couple a solution for transient groundwater flow, by varying precipitation to reflect glacial and interglacial local climate. However, paleoclimate data were limited and the precipitation reconstruction was insufficient for use. Additionally, when precipitation was varied by 25% (the difference between reconstructed LGM average and modern average) over 60,000-yr periods, head variation was found to be ~1.6 % within the modeled region of the aquifer. Given the lack of precipitation data, and the low head variation when using a transient input, a steady-state solution was deemed appropriate. Subsequently, recharge flux was matched to maintain the observed head gradient and groundwater velocity was uniform along the flow path. Mass flux over the modeled period was calculated as:

$$recharge\ flux\ = \left(\frac{RM}{365\times86400}\right)\times\ \rho_w, \tag{5}$$

where *RM* is the mean annual recharge, converted to units of seconds, and ρ_w is the density of water (1000 kg/m^3).

3.3 Isotopic Input

Stable isotopes are reported in ‰ deviation from a standard value of 0, referenced to Vienna Standard Mean Ocean Water (VSMOW), using the δ notation:

$$\delta = ((R_{\text{sample}}/R_{\text{standard}}) - 1) \times 1000, \tag{6}$$

where *R* refers to the isotopic ratio (^{2}H/^{1}H or ^{18}O/^{16}O) of the sample and standard respectively. R_{sample} for ^{18}O/^{16}O of recharge was calculated using equation (6). The result was then multiplied by a constant equal to the average density of water (1000 kg/m^3):

$$Isotope\ Ratio\ = \left(\frac{\delta^{18}O}{1000} + 1\ \right)\times 1000. \tag{7}$$

This converted value of $\delta^{18}O$ was used within the transport model and isotope-flux piecewise function. Calculated values were then converted back into delta notation using:

$$\delta^{18}O = \left(\frac{C_{approx.}}{1000} - 1\right)\times 1000, \tag{8}$$

where *C* is equal to the calculated isotope ratio along the flowpath.

3.4 Model Parameters

3.4.1 Aquifer

Where available, aquifer hydraulic parameters were taken from prior studies within the lower Wilcox (Brahana and Broshears 2001; Pugh 2009) or representative values for the medium lithology (Fetter 2001; Freeze and Cherry 1979). A variety of values were found for hydraulic conductivity *k*; as no spatial trend was apparent, an arithmetic average was calculated. The value of *k* was the same order of magnitude used in the MERAS model (Clark and Hart 2009) and values compiled by Haile (2011), which varied from 1×10^{-3} cm/s to 4.5×10^{-2} cm/s.

3.4.2 Aquitard

No hydraulic characteristics were located for the Midway Group, but none were needed because no flow from one unit to the other was modeled. A diffusive coefficient in a clay-rich medium (Hendry and Wassenaar 1999) was used to represent ^{18}O diffusion in the Midway Group. Table 1 provides a summary of constant model parameters.

Table 1- Model parameters and source.

Parameter	Value	Units	Source
Model Mesh	250	m	
Time Tolerance	0.1		
Aquifer Hydraulic Conductivity	0.00003	m/s	Arithmetic average; Brahana and Broshears 2008; Pugh 2009
Aquifer Thickness	20–400	m	Arbitrary
Aquifer Porosity	0.15–0.225		Castany 1967
Aquitard Porosity	0.35		Castany 1967
^{18}O Diffusion Coefficient	2.27×10^{-9}	m/s	Tanaka 1975
^{18}O Diffusion Coefficient in Clay	1.7×10^{-10}	m/s	Hendry and Wassenaar 1999
Longitudinal Dispersion	$0.83 \times \log(L^*)^{2.414}$	m	Xu and Eckstein 1995

* where L is flowpath length

3.4.3 Initial Conditions

Initial values of head were calculated linearly along the modeled flowpath, assuming a hydraulic head of zero at the lower boundary, as:

$$h(x) = \frac{RM}{kf}(L - x), \quad (9)$$

where *RM* is the mean recharge, k_f is the aquifer hydraulic conductivity, *L* is the flowpath length, and *x* is distance along the flowpath.

As no information on aquitard porewater $\delta^{18}O$ or absolute ages of current lower Wilcox groundwater samples from Haile (2011) was available, an initial value for each had to be approximated. The initial isotope ratio was based on the calculated meteoric $\delta^{18}O$ values of Harmon and Schwarcz (1981) under two assumptions: 1) aquifer water would fall somewhere within the range of calculated values and 2) aquitard values, assuming fluxes both into and out of the aquitard, could approach the mean of prior isotope signals. With that in mind, the mean of the modeled isotope signal or speleothem-based values (Harmon and Schwarcz 1981) were used for aquitard isotope ratio, and the median was used for the aquifer.

3.4.4 Isotope and mass flux

Annual effective recharge (= precipitation – evapotranspiration) reported by Haile (2011) was used as a starting point for recharge. This was adjusted to match the observed head gradient within the lower Wilcox.

Isotope signals were based on speleothem drip water, trends in speleothem $\delta^{18}O$, and inferences based on qualitative proxies (sea level, glaciation, loess and till deposition). Additional isotope signals were based on groundwater velocities inferred from ^{36}Cl and observed $\delta^{18}O$ values within the lower Wilcox (Haile 2011). The ^{18}O flux was calculated as a piecewise function of 5000-yr intervals across the study period (Fig. 11; Appendices A and B). Dates between speleothem-based values were calculated using linear interpolation and qualitative proxies.

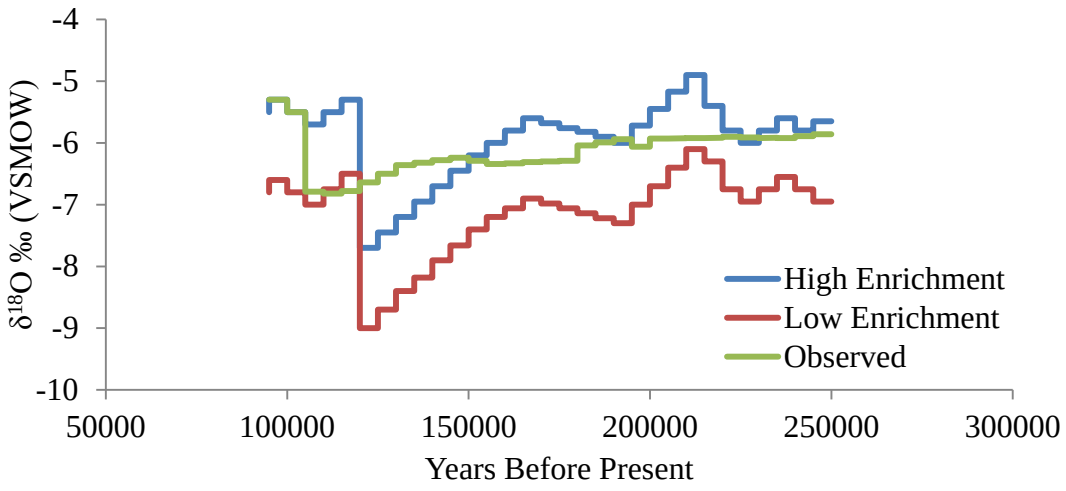

Figure 11 - High enrichment and low enrichment (Harmon and Schwarcz 1981), and Wilcox observed isotope input signals.

Chapter Four

4. Results

4.1 Sensitivity Analysis

A sensitivity analysis was conducted to determine the individual influence of varied groundwater velocity and isotope abundance gradient on the distribution of $\delta^{18}O$ in the aquifer. Groundwater velocity was varied from 1.82×10^{-9} to 2.81×10^{-7} m/s. Aquitard thickness was tested across a range of values from 40 to 400 m. Aquitard isotope abundance was altered from equal to 100× aquifer isotope ratio. Aquifer thickness was maintained at 40 m across all tests. Initial aquitard and aquifer $\delta^{18}O$ values were -4 ‰ and -6 ‰, respectively, except for isotope concentration gradient analysis.

The $\delta^{18}O$ value mid-flowpath is maintained as groundwater velocity increases from the minimum to 1.96×10^{-8} m/s, then fell as velocity increases further (Fig. 12). Aquifer $\delta^{18}O$ is notably higher at lower velocities, with an increase of almost 1 ‰ between the highest velocity and velocities $\leq 10^{-8}$ m/s. The decrease in $\delta^{18}O$ with increasing velocity is likely due to advection transporting water through the aquifer faster than aquitard-aquifer diffusive exchange can alter the isotope ratio. This supports prior work (Hendry and Schwartz 1988; LaBolle et al. 2008) suggesting that diffusive flux from a bounding aquitard is capable of influencing aquifer isotope abundances as velocity decreases. Regression indicates a non-linear trend as best fit across the range of groundwater velocities tested (Fig. 13).

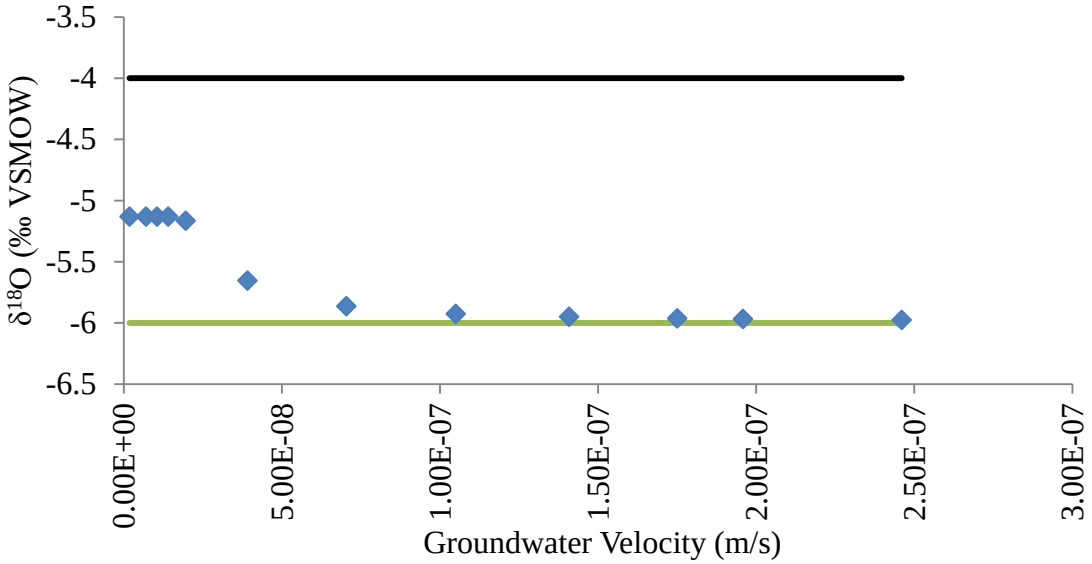

Figure 12 - Aquifer $\delta^{18}O$ vs. groundwater velocity mid-flowpath (150 kyr run time) for cell-centered interaction (0.5bt). Initial $\delta^{18}O$ values for water in the aquifer and aquitard are shown with green and black lines, respectively. $\delta^{18}O$ calculated from modeled aquifer water isotope ratio (Eq. 9). E is equivalent to a factor of 10.

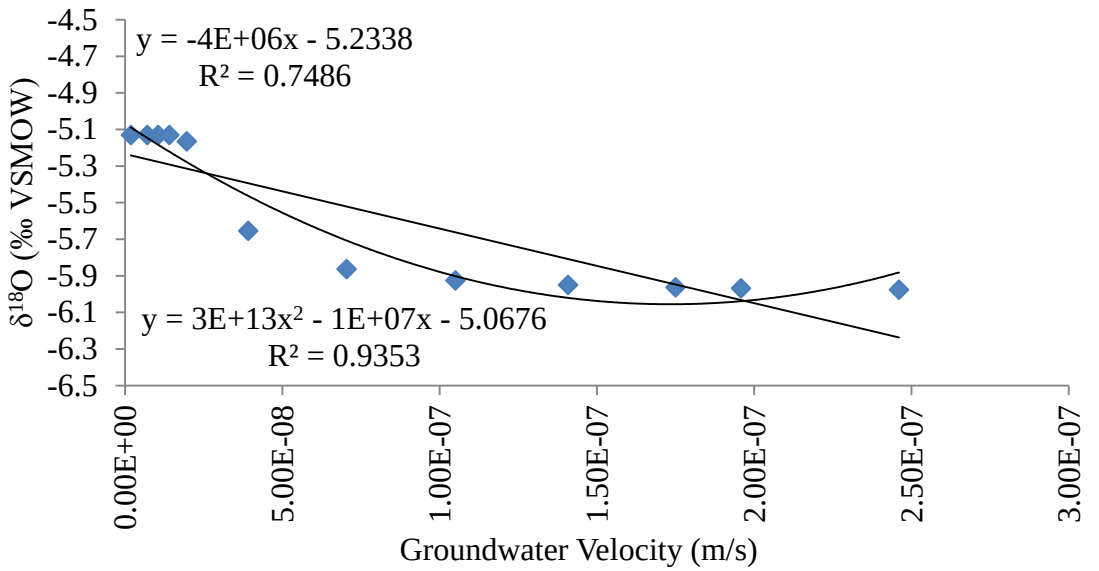

Figure 13 - Aquifer $\delta^{18}O$ vs. groundwater velocity (150 kyr run time), full aquitard thickness interaction, linear and polynomial trends.

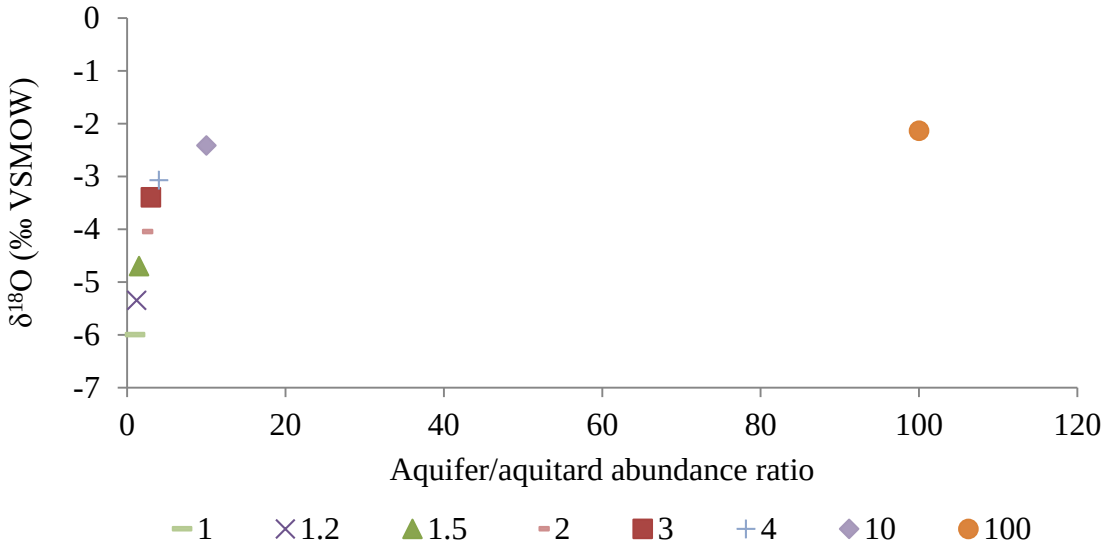

Figure 14 - Aquifer $\delta^{18}O$ vs. ratio of $\delta^{18}O$ in the aquifer versus the aquitard.

Diffusive flux increases with increasing isotope gradient and approaches an asymptotic value once aquitard isotope abundance reaches 4 × aquifer abundance (Fig. 14). LaBolle et al. (2008) also observed the dependence of the diffusive flux on the isotope composition gradient.

4.2 Hypothesis Testing

The effects of varying aquitard interaction thickness and groundwater velocity were also examined for a variable isotope input. The $\delta^{18}O$ values inferred by Harmon and Schwarcz (1981) for speleothem inclusion waters from Kentucky based on the modern GMWL (herein referred to as high enrichment) were input across a 175-kyr runtime. For time periods lacking $\delta^{18}O$ data, input values were calculated using linear interpolation. A mass flux of 0.151 m/yr was maintained unless otherwise noted.

The diffusive flux is greater for full interaction thickness, as shown by greater variation from surface signal isotope values (red vs. orange line; Fig. 15). Increasing the diffusive flux by altering interaction thickness increases dispersive mixing (grey and peach; Fig. 16), while increasing groundwater velocity increases both dispersive mixing and penetration of the surface isotope signal (light blue vs. dark blue and green; Fig. 16).

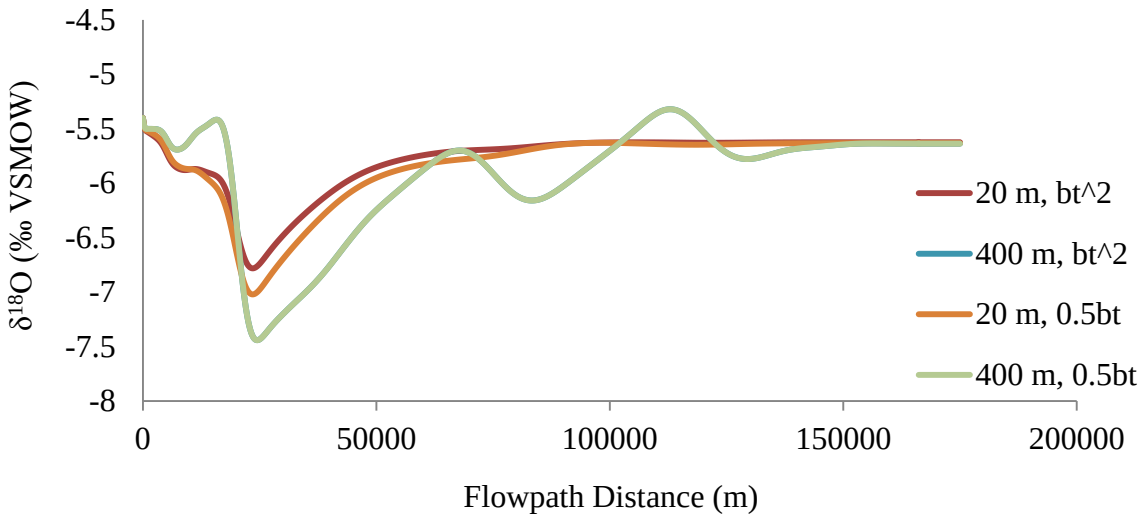

Figure 15 - Aquifer $\delta^{18}O$ vs. flowpath distance for varying aquitard thickness, full (bt^2) and cell-centered (0.5bt) interaction thickness, 0.151 m/yr mass flux, high enrichment signal with diffusion.

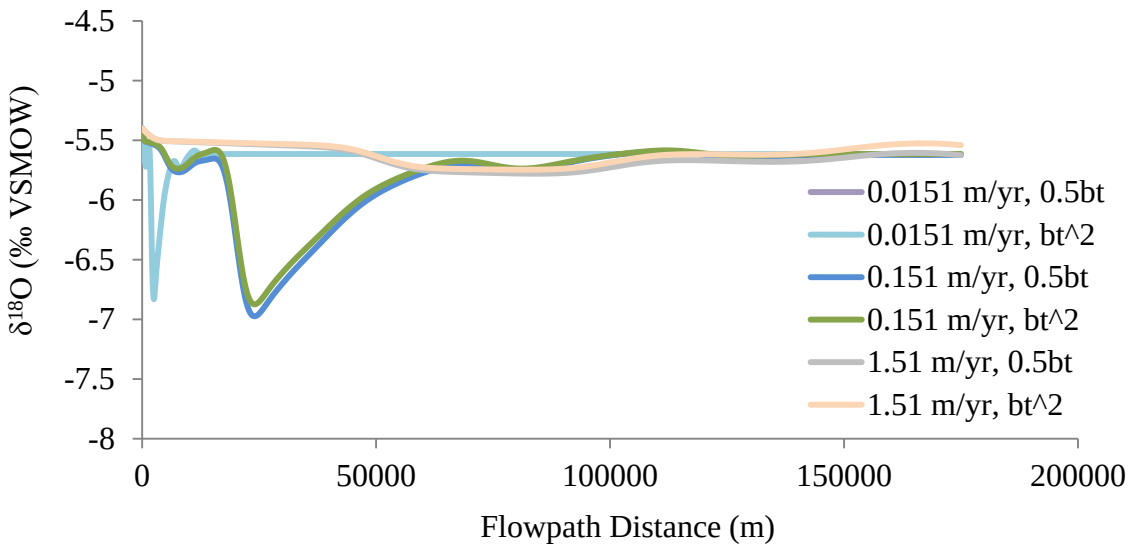

Figure 16 - Aquifer $\delta^{18}O$ vs. flowpath distance, varied flux, full (bt^2) and cell-centered (0.5bt) interaction thickness, 40-m aquitard thickness, high enrichment with diffusion.

4.3 Scenario and Wilcox-Specific Testing

Using observed lower Wilcox $\delta^{18}O$ as a surface signal gives a reasonable post-fault approximation, assuming ^{36}Cl-derived groundwater travel time to the fault is appropriate (Fig. 17). A recharge flux of 0.17 m/yr (groundwater velocity of 3.55×10^{-8} m/s), which is slightly greater than both head-calibrated recharge (0.14 m/yr; groundwater velocity of 2.96×10^{-8} m/s) and effective recharge (0.15 m/yr; groundwater velocity of 3.15×10^{-8} m/s), provides the best approximation (Fig. 17; light blue).

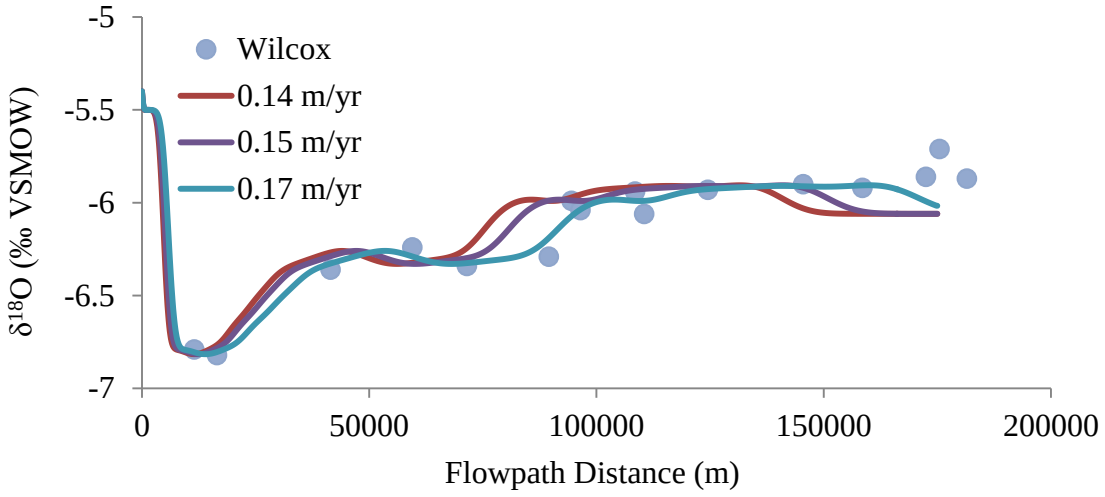

Figure 17 - Aquifer $\delta^{18}O$ vs. flowpath distance, with initial aquifer $\delta^{18}O$ equal to -6.06 ‰ (median), isotope input equal to observed Wilcox signal without diffusion, and mass fluxes of 0.14, 0.15, and 0.17 m/yr.

Under the same conditions, with a diffusive flux and a 0.15 m/yr mass flux, the surface signal is smoothed and, maintaining the condition of aquitard concentration equal to the mean of the aquifer, aquifer isotope ratio is shifted away from observed (Fig. 18).

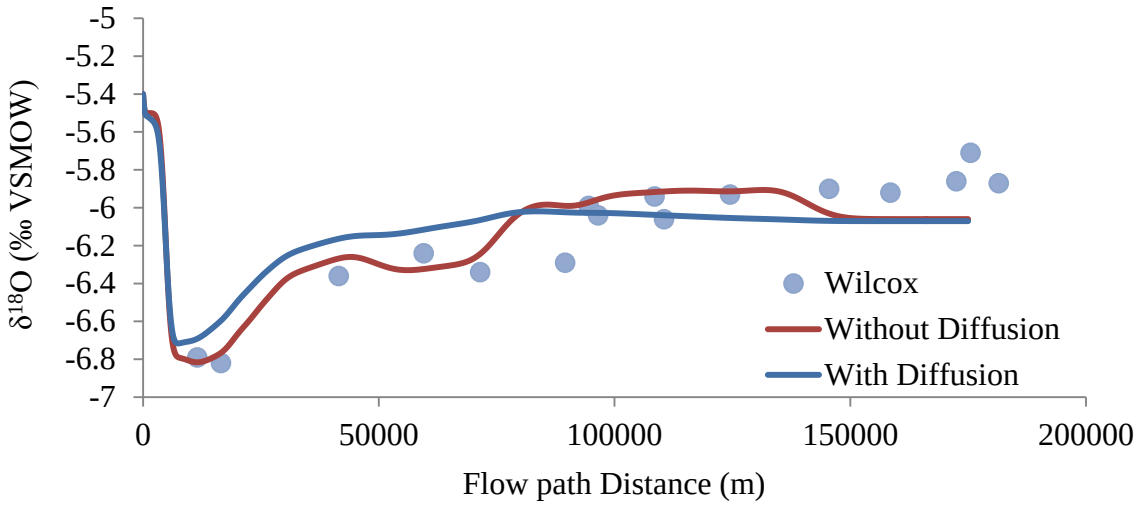

Figure 18 - Aquifer $\delta^{18}O$ vs. flowpath distance, with initial aquifer $\delta^{18}O$ equal to -6.06 ‰ (median), isotope input equal to observed Wilcox signal without diffusion, 0.15 m/yr mass flux without (red) and with diffusion (blue).

4.4 Speleothem-Based Isotope Input

High- and low-enrichment (following the paleo-GMWL of Harmon and Schwarcz [1981]) isotope signals were initially tested for head-calibrated, steady-state mass flux. Initial conditions and the $\delta^{18}O$ surface signal were adjusted based on observed results. A low-enrichment isotope signal with varying initial aquifer and aquitard conditions can be made to approach the observed lower Wilcox signal with significant aquitard enrichment (Fig. 19; light blue). However, fault proximal isotope values are significantly lower than observed assuming interpolation between wells is accurate (Fig. 19; green).

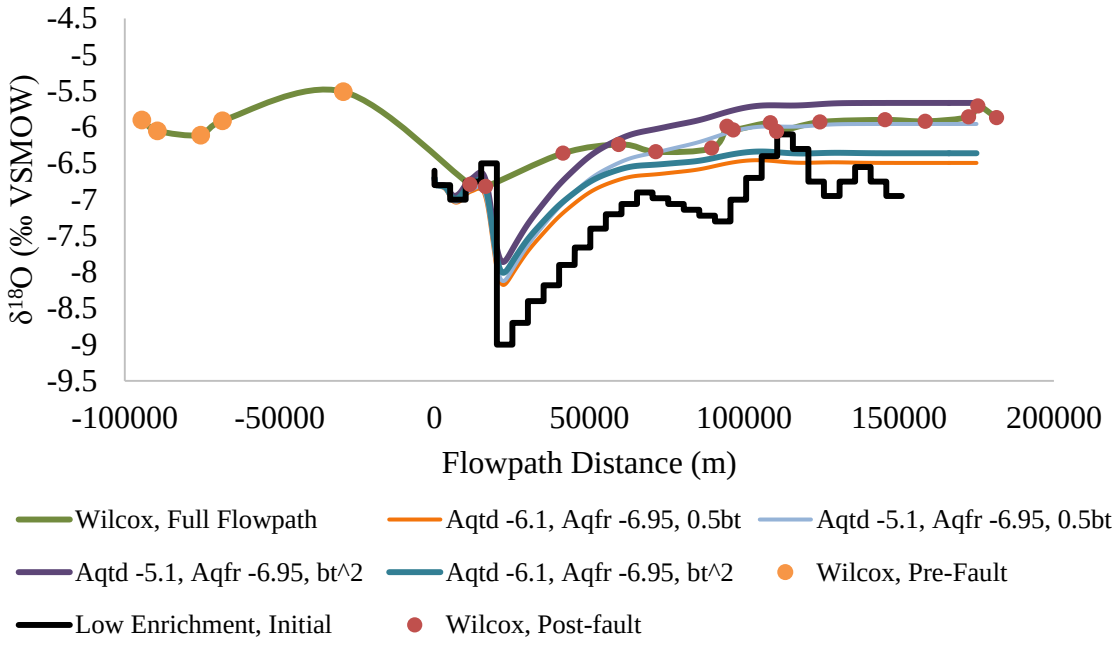

Figure 19 - Aquifer $\delta^{18}O$ vs. flowpath distance, under varied isotope gradient, full (bt^2) and cell-centered aquitard interaction thickness (0.5bt), 40-m aquitard thickness, 0.14 m/yr mass flux, using low enrichment signal with diffusion. Advective transport of low enrichment signal is shown in black; fault located at 0 m flowpath distance.

The high-enrichment isotope signal with varied initial aquifer and aquitard conditions can also be made to approach the observed signal (Fig. 20a, b, c). Modeled $\delta^{18}O$ values are generally more enriched than observed values unless a diffusive flux into the aquifer is created (Fig. 20c; pink and light green curves). Varying the high-enrichment signal brings results closer to observed, with the diffusive flux acting to reduce variability within the signal. However, the modeled signal, while reproducing the general trend of a significant drop in $\delta^{18}O$ immediately down-gradient from the fault followed by a gradual down-gradient increase, cannot closely match the observed signal using selected model parameters.

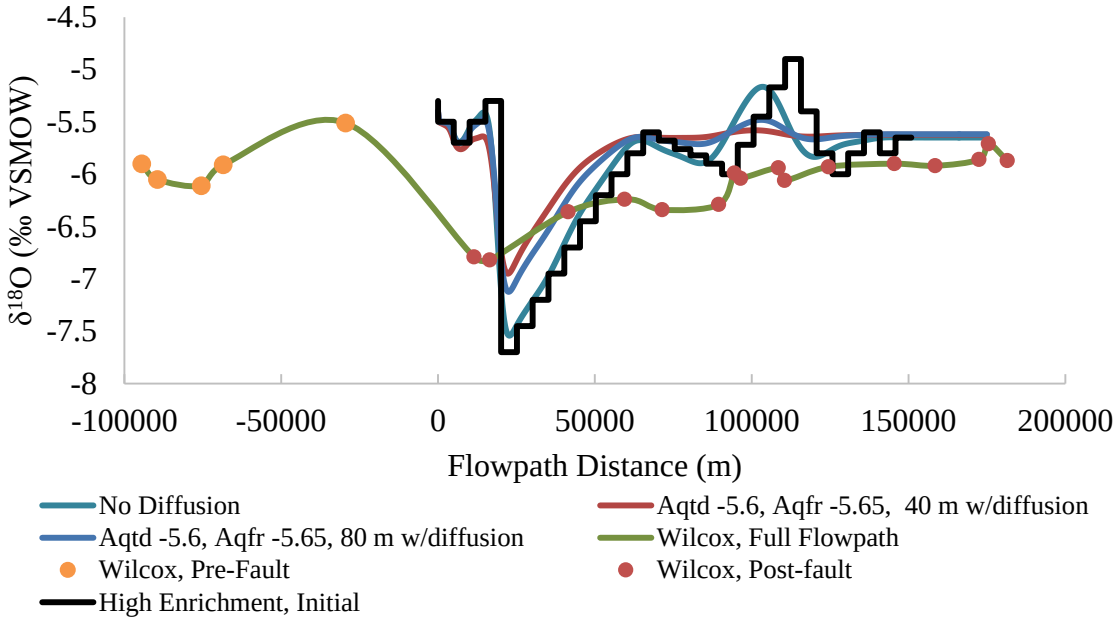

Figure 20a

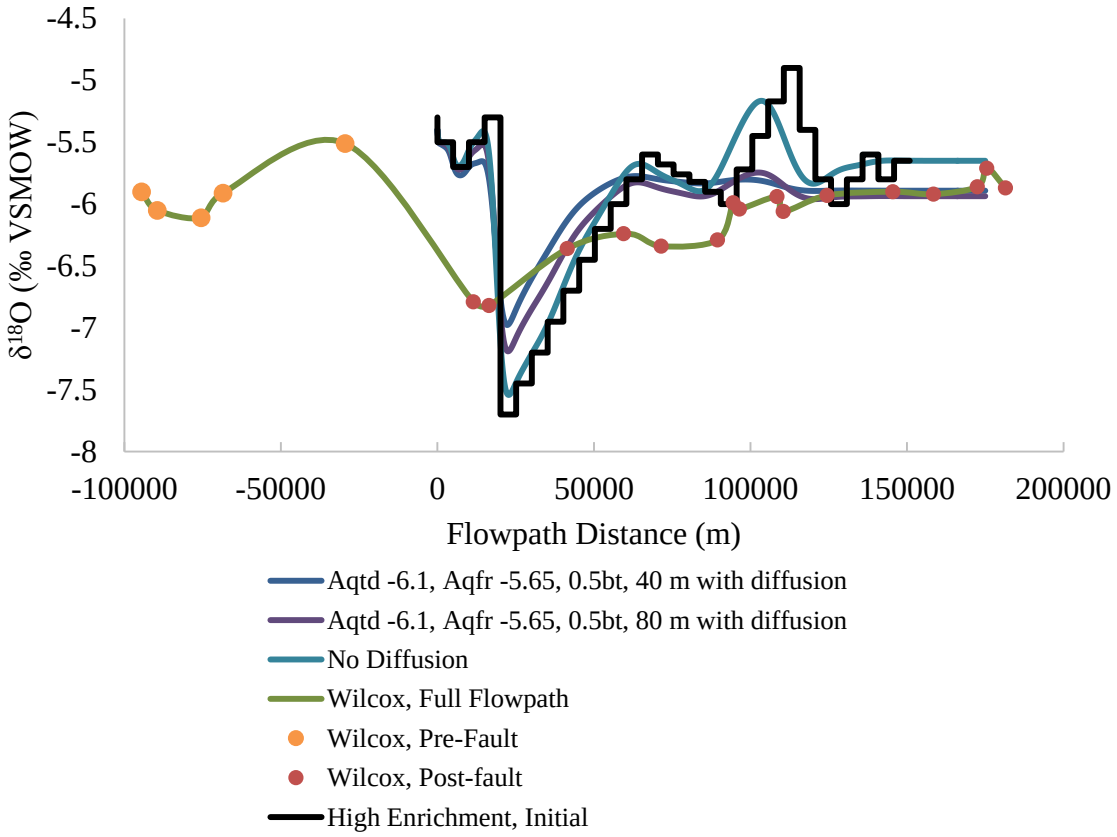

Figure 20b

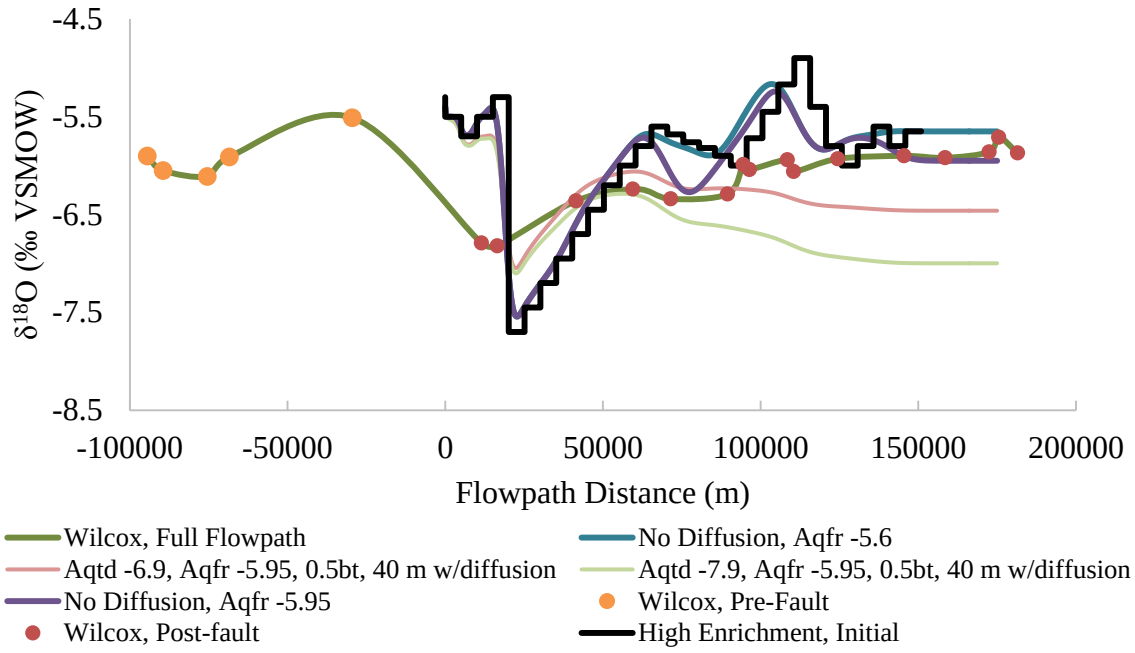

Figure 20c

Figure 20a, b, c - Aquifer $\delta^{18}O$ vs. flowpath distance, high enrichment, full (bt^2) and cell-centered aquitard interaction thickness (0.5bt), 0.14 m/yr mass flux, varied gradient. Advective transport of high enrichment signal is shown in black; fault located at 0 m flowpath distance.

Chapter Five

5. Discussion and Conclusions

Paleoclimate and paleowater $\delta^{18}O$ data were difficult to locate for the study area and a limited number of data points, with varying degrees of dating precision, were used to inform the approximate isotope signal. The model provides a reasonable approximation of the observed signal, barring a lack of full surface-signal $\delta^{18}O$ penetration, for the selected parameters when the observed lower Wilcox signal is used as input. Additionally, the added diffusive flux generally behaves as expected, with aquifer isotope ratio responding appropriately to variations in isotope concentration gradient. However, when using approximated paleoclimate and paleowater isotope ratios, the model does not closely match the observed isotope signal. The hydraulic parameters of the aquifer are in agreement with prior work, and groundwater velocity has been calculated to the same order of magnitude as indicated by Haile (2011). Assumptions regarding upper boundary conditions, flow conditions (in particular, the assumption of uniform velocity), and the 1-D geometry of the model all likely limit the goodness of the match.

Nonetheless, the general observed trend, a significant drop in $\delta^{18}O$ across the fault and then a gradual increase to a maximum down the flowpath, is reproduced. Addition of a diffusive flux was found both to influence $\delta^{18}O$ of groundwater in the aquifer, enriching or depleting it depending upon the isotopic gradient, and to smooth the surface signal by reducing variability. Sensitivity analyses suggest that as groundwater velocity approaches 10^{-8} m/s or less, a diffusive flux into or from a bounding aquitard can influence $\delta^{18}O$ of groundwater in the aquifer. However, if a diffusive flux is influencing the isotopic composition of aquifer waters, then $\delta^{18}O$ should increase or decrease with proximity to the aquitard. A plot of $\delta^{18}O$ vs. distance from the Midway Group contact (Fig. 21) shows no clear trend.

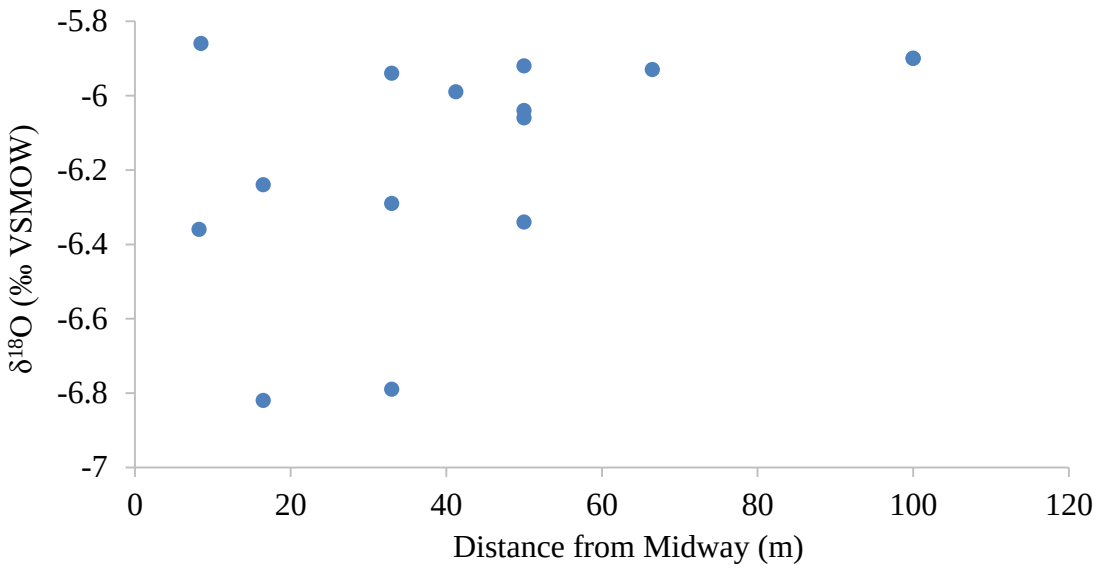

Figure 21 - $\delta^{18}O$ vs. inferred distance from Midway Group contact (from data of Haile [2011]).

Another possible explanation for the progressive enrichment in ^{18}O along the lower Wilcox post-fault flowpath is cross-formational leakage from an underlying or overlying aquifer. The deeper McNairy aquifer, separated from the lower Wilcox by the Midway, is not significantly depleted relative to the Wilcox (Brahana and Mesko 1985). Enrichment in the lower Wilcox decreases with increasing latitude, which is consistent with Rayleigh distillation as air masses originating over the Gulf of Mexico move northward and progressively rain out the heavier isotope (^{18}O or ^{2}H) (Haile 2011). Dutton et al. (2005) derived the following relationship between latitude (LAT) and $\delta^{18}O$ of modern precipitation for stations in the conterminous USA at elevations < 200 m above mean sea level:

$$\delta^{18}O = -0.0057LAT^2 + 0.1078LAT - 1.6544 \ (r^2 = 0.80) \qquad (10)$$

However, the slope of this empirical relationship is markedly less than the observed relationship along the lower Wilcox post-fault flowpath (Fig. 22), and there is not independent hydraulic or geochemical evidence for progressive downward leakage along the flowpath.

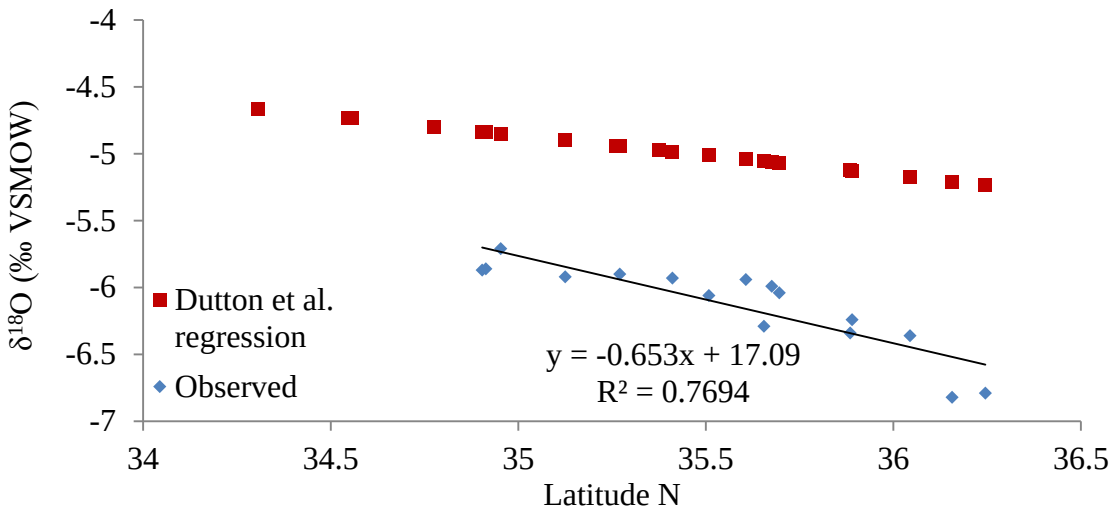

Figure 22 - Observed lower Wilcox $\delta^{18}O$ (Haile 2011) and inferred $\delta^{18}O$ trend of modern precipitation (Dutton et al. 2005) vs. latitude.

There is evidence of possible downward, relatively rapid leakage along faults in the New Madrid Seismic Zone. Brahana and Mesko (1985) reported the co-occurrence of detectable ^{3}H (2 pCi/L) and low ^{14}C (8.1% modern C) for a 398-m-deep lower Wilcox well at Hayti, Missouri (~ 30 km SSW of the Reelfoot Thrust and ~10 km WNW of the Axial Fault [Guo et al., 2014]). Isotopically depleted groundwater could be attributed to infiltration of melt-water pulses moving down the Mississippi River valley from the Laurentide Ice Sheet (Clayton et al. 1966), as recorded in Gulf of Mexico sea floor sediments at 14, ~120, and 210 ka (Joyce et al. 1993). However, a significant flux would be required to attain the observed $\delta^{18}O$ minimum of -6.82 ‰. Assuming binary mixing of upgradient groundwater with $\delta^{18}O$ of -5.8 ‰ and melt water with $\delta^{18}O$ of -10 ‰ (Clayton et al. 1966), melt water would have to comprise 24% of groundwater downgradient of the fault zone, which is improbable.

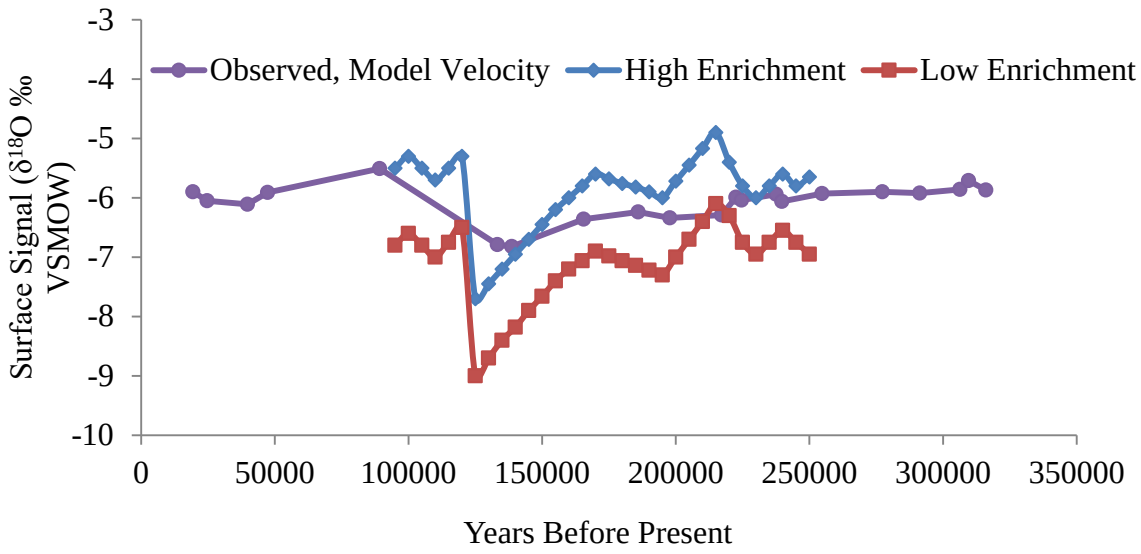

Figure 23 - $\delta^{18}O$ (Harmon and Schwarcz 1981; Haile 2011) vs. recharge date using speleothem U/Th dates and velocity derived from ^{36}Cl residence time.

It appears that $\delta^{18}O$ behavior along flowpaths in regional aquifers falls along a continuum, depending upon the isotopic signal and timing of recharge and the hydraulics of the aquifer. In the lower Wilcox, diffusion and cross-formational flow may affect the isotopic signal, but diffusion does not appear to have caused differential enrichment of O and H isotopes, as indicated by the fact that a plot of $\delta^{18}O$ vs. $\delta^{2}H$ values falls along the local meteoric water line (Haile 2011, Fig. 4.7). Enrichment down the flowpath primarily appears to reflect temporal variability in paleorecharge, as indicated by the speleothem inclusion water data of Harmon and Schwarcz (1981) (Fig. 23). By comparison, Plummer et al. (2012) demonstrated a clear divide in $\delta^{18}O$ abundance at the end of the LGM within the lower Patapsco aquifer in Maryland (Fig. 1), whereas Hendry and Schwartz (1988) presented a pattern of down-gradient ^{18}O enrichment in the Milk River aquifer in Alberta. These differences in $\delta^{18}O$ distributions are not simply a function of groundwater velocity: for all three aquifer systems, velocity is on the order of 10^{-8} to 10^{-9} m/s (based on ^{36}Cl data for the Patapsco and lower Wilcox and on groundwater-flow modeling for the Milk River). Nonetheless, the possible interplay between groundwater velocity and the diffusive flux is intriguing. This suggests that along flowpaths with residence times on the order of 10^{5} years, variation in $\delta^{18}O$ paleorecharge signals may be reduced by diffusion into and out of bounding low-permeability units, as well as by mechanical dispersion.

Appendices

Appendix A: Observed isotope values by well (Haile 2011)

Well ID	Town	Distance from Recharge (km)	Depth to Midway (m)	$\delta^{18}O$ (‰ VSMOW)	$\delta^{2}H$ (‰ VSMOW)	Depth Below Land Surface (m)
2		18		-5.9	-35.94	45.1
1		23		-6.05	-36.18	19.2
3	Sikeston, MO	37		-6.11	-36.97	23.4
4		44		-5.91	-35.15	89.9
5	Parma, MO	83		-5.51	-33.13	58.5
28		99		-6.14	-32.45	190.5
6	Hayti, MO	124	33	-6.79	-41.31	313.3
7		129	16.5	-6.82	-39.41	333.4
8		154	8.25	-6.36	-37.82	336.5
9		173	16.5	-6.24	-36.94	350.5
10		184	50	-6.34	-35.7	279.8
13		202	33	-6.29	-35.33	382.5
12		207	41.25	-5.99	-35.18	372.5
11		209	50	-6.04	-34.9	356.6
14		221	33	-5.94	-34.16	378
15		223	50	-6.06	-35.49	409.4
16		237	66.5	-5.93	-34.12	393.5
17		258	100	-5.9	-33.74	452.7
18		271	50	-5.92	-33.6	422.4
20		285	8.5	-5.86	-32.74	438
19		288		-5.71	-33.06	426.1
21		294		-5.87	-35.15	428

Appendix B: High and low isotope enrichment model inputs (Harmon and Schwarcz 1981)

Years Before Present	Input Time Step	High Enrichment ($\delta^{18}O$, ‰ VSMOW)	Low Enrichment ($\delta^{18}O$, ‰ VSMOW)
250000	0	-5.65	-6.95
245000	5000	-5.8	-6.75
240000	10000	-5.6	-6.55
235000	15000	-5.8	-6.75
230000	20000	-6	-6.95
225000	25000	-5.8	-6.75
220000	30000	-5.4	-6.3
215000	35000	-4.9	-6.1
210000	40000	-5.17	-6.4
205000	45000	-5.45	-6.7
200000	50000	-5.72	-7
195000	55000	-6	-7.3
190000	60000	-5.9	-7.22
185000	65000	-5.82	-7.14
180000	70000	-5.76	-7.06
175000	75000	-5.68	-6.98
170000	80000	-5.6	-6.9
165000	85000	-5.8	-7.06
160000	90000	-6	-7.2
155000	95000	-6.2	-7.4
150000	100000	-6.45	-7.66
145000	105000	-6.7	-7.9
140000	110000	-6.95	-8.18
135000	115000	-7.2	-8.4
130000	120000	-7.45	-8.7
125000	125000	-7.7	-9
120000	130000	-5.3	-6.5
115000	135000	-5.5	-6.75
110000	140000	-5.7	-7
105000	145000	-5.5	-6.8
100000	150000	-5.3	-6.6
95000	155000	-5.5	-6.8

REFERENCES

Brahana JV, Broshears RE (2001) Hydrogeology and ground-water flow in the Memphis and Fort Pillow aquifers in the Memphis area, Tennessee. US Geol Surv Water-Resour Invest Report 89-4131

Brahana JV, Mesko TO (1985) Hydrogeology and preliminary assessment of regional flow in the Upper Cretaceous and adjacent aquifers in the northern Mississippi Embayment. US Geol Surv Water Resour Invest Rep 87-4000

Bromwich DH, Toracinta ER, Oglesby RJ, Fastook JL, Hughes TJ (2005) LGM summer climate on the southern margin of the Laurentide ice sheet: wet or dry? J Clim 18(16):3317–3338

Clark B, Hart R (2009) The Mississippi Embayment Regional Aquifer Study (MERAS): documentation of a groundwater-flow model constructed to assess water availability in the Mississippi Embayment. US Geol Surv Sci Invest Rep 2009-5172

Castany G (1967) Traité pratique des eaux souterraines. Dunod, Paris

Clayton RN, Friedman I, Graf DL, Mayeda TK, Meents WF, Shimp NF (1966) The origin of saline formation waters - 1. Isotopic compositions. J Geophys Res 71(16):3869–3882

Darling GW, Bath AH, Gibson JJ, Rozanski K (2005) Isotopes in water. In: Isotopes in palaeoenvironmental research. Springer, Dordrecht, pp 1 - 66

Davis MB, Shaw RG (2001) Range shifts and adaptive responses to Quaternary climate change. Science 292:673–679

Denniston RF, Dupree M, Dorale JA, Asmerom Y, Polyak VJ, Carpenter SJ (2007) Episodes of late Holocene aridity recorded by stalagmites from Devil's Icebox Cave, central Missouri, USA. Quat Res 68:45–52

Dorale JA, Edwards RL, Ito E, Gonzalez LA (1998) Climate and vegetation history of the midcontinent from 75 to 25 ka: a speleothem record from Crevice Cave, Missouri, USA. Science 282:1871–1874

Dutton A, Wilkinson BH, Welker JM, Bowen GJ, Lohmann KC (2005) Spatial distribution and seasonal variation in $^{18}O/^{16}O$ of modern precipitation and river water across the conterminous USA. Hydrol Process 19:4121–4146

Dyke AS, Prest VK (1987) Late Wisconsinan and Holocene history of the Laurentide Ice Sheet. Géogr Phys Quat 41:237–263

Fetter CW (2001) Applied hydrogeology. Prentice-Hall, Upper Saddle River

Forman SL, Pierson J (2002) Late Pleistocene luminescence chronology of loess deposition in the Missouri and Mississippi river valleys, United States. Paleogeogr Palaeoclimatol Palaeoecology 186:25–46

Freeze RA, Cherry JA (1979) Groundwater. Prentice-Hall, Eaglewood Cliffs

Friedman I, O'Neil JR (1977) Compilation of stable isotope fractionation factors of geochemical interest. US Geol Surv Prof Pap 440-KK

Guo L, Magnani MB, McIntosh K, Waldron B (2014) Quaternary deformation and fault structure in the northern Mississippi Embayment as imaged by near-surface seismic reflection data. Tectonics 33:807–823

Haile E (2011) Chemical evolution and residence time of groundwater in the Wilcox aquifer of the northern Gulf Coastal Plain. PhD Dissertation, University of Kentucky, Lexington

Harmon RS, Schwarcz HP (1981) Changes of ^{2}H and ^{18}O enrichment of meteoric water and Pleistocene glaciation. Nature 290:125–128

Hart RM, Clark BR, Bolyard SE (2008) Digital surfaces and thicknesses of selected hydrogeologic units within the Mississippi Embayment Regional Aquifer Study (MERAS): US Geol Surv Sci Invest Rep 2008-5098

Hendry MJ, Schwartz FW (1988) An alternative view on the origin of chemical and isotopic patterns in groundwater from the Milk River aquifer, Canada. Water Resour Res 24:1747–1763

Hendry MJ, Wassenaar LI (1999) Implications of the distribution of δD in pore waters for groundwater flow and the timing of geologic events in a thick aquitard system. Water Resour Res 35:1751–1760

Hosman RL (1996) Regional stratigraphy and subsurface geology of Cenozoic deposits, Gulf Coastal Plain, south-central United States. US Geol Surv Prof Pap 1416-G

Joyce JE, Tjaisma LRC, Prutzman JM (1993) North American glacial meltwater history for the past 2.3 m.y.: oxygen isotope evidence from the Gulf of Mexico. Geology 21:483–486

Kim SJ, Crowley TJ, Erickson DJ, Govindasamy B, Duffy PB, Lee BY (2006) High-resolution climate simulation of the last glacial maximum. Climate Dynam. 31:1–16

LaBolle EM, Fogg GE, Eweis JB, Gravner J, Leaist DG (2008) Isotopic fractionation by diffusion in groundwater, Water Resour Res 44(7):W070405.

Markewich HW, Wysocki DA, Pavich MJ, Rutledge EM, Millard Jr. HT, Rich FJ, Maat PB, Rubin M, McGeehin JP (1998) Paleopedology plus TL, ^{10}Be, and ^{14}C dating as tool in stratigraphic and paleoclimatic investigations, Mississippi River Valley, U.S.A. Quat Int 51/52:143–167

Missouri Climate Center (2016) Missouri average summer temperature. University of Missouri, http://climate.missouri.edu/charts/chart4.php. Accessed 31 March, 2016

Muhs DR, Wehmiller JF, Simmons KR, York LL (2003a) Quaternary sea level history of the U.S. In: The Quaternary period in the United States. Elsevier, Amsterdam, pp 147–183

Muhs DR, Ager TA, Bettis III EA, McGeehin J, Been JM, Begét JE, Pavich MJ, Stafford Jr TW, De Anne SP (2003b) Stratigraphy and paleoclimate significance of Late Quaternary loess-paleosol sequences of the last interglacial-glacial cycle in central Alaska. Quat Sci Rev 22:1947–1986

O'Neil, J R, Taylor Jr, HP (1969) Oxygen isotope equilibrium between muscovite and water, J. Geophys. Res., 74(25):6012-6022

Plummer LN, Eggleston JR, Raffensperger J, Hunt AG, Casile GC, Andreasen DC (2012) Old groundwater in parts of the upper Patapsco aquifer, Atlantic Coastal Plain, Maryland, USA: evidence from radiocarbon, chlorine-36 and helium-4. Hydrogeol J 20(7):1269–1294.

Pugh AL (2009) Potentiometric surfaces and water-level trends in the Cockfield (upper Claiborne) and Wilcox (lower Wilcox) aquifers of southern and northeastern Arkansas, 2009. US Geol Surv Sci Invest Rep 2010-2014

Rodbell DT, Forman SL, Pierson J, Lynn WC (1997) Stratigraphy and chronology of Mississippi Valley loess in western Tennessee. Geol Sci Am Bull 109:1134–1148

Rovey II CW, Balco G (2011) Summary of early and middle Pleistocene glaciations in northern Missouri, USA. In: Quaternary glaciations—extent and chronology. Elsevier, Amsterdam, pp 553–561

Tanaka K (1974) Measurements of self-diffusion coefficients of water in pure water and in aqueous electrolyte solutions. J Chem Soc Faraday Trans 71:1127–1131

Voelker SL, Stambaugh MC, Guyette RP, Feng X, Grimley DA, Leavitt SW, Panyushkina I, Grimm EC, Marsieck JP, Shuman B, Curry BB (2015) Deglacial hydroclimate of midcontinental North America. Quat Res 83:336–344

Wackerbarth, AK (2012) Towards a better understanding of climate proxies in stalagmites - Modelling processes from surface to cave. [Ph.D thesis]: University of Heidelberg, 149 p.

Williams JW, Shuman BN, Webb III T (2001) Dissimilarity analyses of late-Quaternary vegetation and climate in eastern North America. Ecology 82(12):3346–3362

Williamson AK, Grubb HF (2001) Ground-water flow in the Gulf Coast aquifer systems, south-central United States. US Geol Surv Prof Pap 1416-F

Xu M, Eckstein Y (1995) Use of weighted least-squares method in evaluation of the relationship between dispersivity and field scale. Ground Water 33: 905–908

Vita

Degrees:
Bachelor of Science in Earth and Atmospheric Science – Geological Sciences and Development Sociology, Cornell University, Cum Laude, December 2011

Associate in Science – Math and Science, State University of New York - Tompkins Cortland Community College, May 2008

Publications:
Currens, Benjamin. 2014. Common Hazards in Karst Terrain (AEN-126). University of Kentucky College of Agriculture, Food and Environment Cooperative Extension Service.

Geisler, Charles and Benjamin Currens. 2015. Impediments to Inland Resettlement under Conditions of Accelerated Sea Level Rise. Manuscript in review.

Geisler, Charles and Benjamin Currens. 2014. Peak Farmland: Revealed Truth or Recreancy? Research in Social Problems and Public Policy. Vol.21, 2014

Benjamin J. Currens